UNITED STATES DEPARTMENT OF THE INTERIOR

GEOLOGICAL SURVEY

Petrology, Geochemistry, and Origin of the Red Mountain Ultramafic Body near Seldovia, Alaska

By

Margo I. Toth

Open-File Report 81-514
1981

Contents

Illustrations

Page

Tables

Petrology, geochemistry, and origin of the Red Mountain ultramafic body near Seldovia, Alaska

by

Margo I. Toth

ABSTRACT

The Red Mountain ultramafic body crops out 13 km southeast of Seldovia, on the southwestern Kenai Peninsula, Alaska, and has been emplaced into the Seldovia Bay complex, a Late Cretaceous subduction unit. The pluton was discordantly intruded in the solid state into sheared and chaotic sequences of graywacke, slate, chert, and limestone metamorphosed to the prehnite-pumpellyite facies. Contacts dip steeply inward and sheared serpentinite is present around the entire margin. Well-developed, primary igneous layering has been folded to form a southwest-plunging synform.

The rocks exposed at Red Mountain consist of layered dunite, wehrlite, and trace amounts of clinopyroxenite, chromitite, serpentinite, and dike rock of varying composition. Garnet clinopyroxenite occurs in aligned strongly foliated lens-shaped masses with serpentinite margins. Relict orthocumulus textures in the chromitite and the presence of primary igneous layering indicates that the bulk of the rocks were formed by cumulus processes. Superimposed on the primary textures are metamorphic deformational features, including the development of kink bands in olivine, recrystallization and polygonalization of olivine grains, and extreme granulation and cataclasis of garnet. The garnet clinopyroxenites show the maximum degree of deformation, followed by the dunites and wehrlites.

Major-element chemistry of the dunite and wehrlite shows a restricted compositional range typified by low Na_2O+K_2O (0.05 percent) and low Al_2O_3 (1 percent). Olivine is unzoned and shows a median composition of Fo_{86} in the

dunite and Fo_{84} in the wehrlite. In the wehrlite, diopside is characterized by high Ca-Ca+Mg atomic ratios (0.57-0.59) and contains no Al_2O_3. In the garnet clinopyroxenites, diopside has Ca-Ca+Mg ratios of 0.67-0.69 and contains 7-8 percent Al_2O_3. Garnet has an unusual composition, dominated by pyrope (33-36 percent), subequal amounts of grossular and almandine (24-29 percent), and lesser amounts of andradite (9-12 percent). Trace-element chemistry shows anomalously high values of chromium and nickel in the dunites and wehrlites.

The Red Mountain pluton is here interpreted to have formed at an oceanic spreading center as a part of an ophiolite sequence, and was emplaced in a Late Cretaceous episode of subduction. The Red Mountain ultramafic body originated as a part of the lower ultramafic cumulate section of the ophiolite. The garnet pyroxenite bodies most likely represent inclusions from the upper mantle. Temperatures of deformation for the pluton may have reached 450°C for representative geological strain rates of 10^{-14}/second, and probably occurred concomitant with subduction and emplacement of the body.

ACKNOWLEDGMENTS

I would like to acknowledge Ed MacKevett, Bill Greenwood, and Jim Munoz for suggestions and encouragement of this report in its thesis state. I thank Don Grybeck for his donation of samples and chemical analyses. Mary Allen provided valuable help as a field assistant in June 1977. Sandy Gunow and Steve Ludington lent assistance on the microprobe at the U.S. Geological Survey in Denver. I would also like to acknowledge Lori Glassgold, Jane Selverstone, and Holly Morris who assisted in drafting the figures.

CHAPTER I

INTRODUCTION

Objectives

The prime objective of this thesis is to determine the origin of the Red Mountain ultramafic body and to further the state of knowledge concerning ultramafic bodies in southern Alaska. A secondary objective is to compare the Red Mountain body to other chromite-rich ultramafic bodies emplaced in similar tectonic regimes in southern Alaska. This comparison may facilitate future chromite exploration programs in southern Alaska.

Procedure

Fieldwork was accomplished in June and August of 1977. Topographic maps at a scale of 1:63,360 were photographically enlarged to a scale of 1:12,000 for detailed geologic mapping. Aerial photographs were used primarily for mapping contact relations and interpreting structural features. As a geologic map had been previously compiled by Guild (1942), the purpose of the fieldwork was to verify his map, to map critical areas in greater detail, to collect samples, and to obtain additional structural data.

Whole-rock major-oxide wet chemical analyses were obtained on many of the samples. These analyses by the U.S. Geological Survey were done according to the techniques outlined by Shapiro (1967, 1975). Standard six-step 30-element semiquantitative emission spectrographic analyses were also obtained from the U.S. Geological Survey according to the method of Grimes and Marranzino (1968) as were atomic absorption analyses on chromium and nickel and fire assay on the trace elements platinum, palladium, rhodium, ruthenium, and iridium.

Individual mineral species were chemically analyzed using an Applied Research Laboratories six-channel electron microprobe. All analyses were on carbon-coated, polished thin sections and several grains of each mineral were

analyzed. A combination of the Energy Dispersive System (EDS) and Wavelength Dispersive System (WDS) was used at an excitation voltage of 15 kV (kilovolts). Sample current was 15 nanoamps and beam current was monitored for 15 seconds. Elements analyzed with the EDS were Al, Si, Ca, Ti, Fe, and Cr. Elements analyzed with the WDS were Mg and K; Mg was analyzed with a KAP (potassium acid phthalate) crystal and K was analyzed with PET (penterythritol) crystal. U.S. Geological Survey olivine and pyroxene group standards were utilized.

This project was accomplished in partial fulfillment of the requirements for the master's degree in geology from the University of Colorado, Boulder, under the direction of Professor James Munoz.

Previous Work

As the ultramafic rocks of Red Mountain contain possible economic chromite deposits, work in the past has focused on the location and nature of the chromite bodies. Grant and Higgins (1910) were the first to write about the deposits, and their work was followed by a thorough study of the geology and chromite deposits of the Kenai Peninsula by Martin and others (1915). Mertie (1919) published further data on the chromite at Red Mountain, and Gill (1922) was the first to publish a map of Red Mountain showing the general geology and location of the chromite deposits. Guild (1942) compiled a detailed geologic map of Red Mountain and included in his report detailed megascopic descriptions of the ultramafic rocks enclosing the chromite ore.

Rutledge (1946) published work concerning the chromite deposits at Red Mountain. Since his report, no other studies were completed on Red Mountain itself until the petrologic study by Forbes and Swainbank (1974) on garnet pyroxenite bodies found within the Red Mountain dunite.

On a regional scale, several papers have been presented concerning the tectonics of the Kenai Peninsula and southern Alaska. Forbes and Lanphere (1973) dated blueschists found near Seldovia and discussed their tectonic significance. Cowan and Boss (1978) presented work on the tectonic framework of the southwestern Kenai Peninsula, and Moore and Connelly (1977) studied the Mesozoic tectonics of the southern Alaskan margin. To the southwest of Red Mountain, Carden and others (1977) and Connelly (1978) studied the deposits on Kodiak Island and correlated them to those found near Red Mountain.

Geographic Setting

The Red Mountain ultramafic body is located approximately 13 km southeast of Seldovia on the southwestern Kenai Peninsula, Alaska (fig. 1). Red Mountain stands as the highest point of the ultramafic body at an elevation of 1,074 m; the lowest point is in the Windy River at an elevation of 296 m. The summit of Red Mountain forms a horseshoe-shaped ridge that opens toward the north of the Windy River valley. The Windy River flows north, then northeast to join the Rocky River, which flows south and empties into Rocky Bay (fig. 2). The ultramafic mass is also drained by minor tributaries of the Seldovia River which flow northwest into Seldovia Bay and by tributaries of Barbara Creek which also flow northwest and drain into Katchemak Bay.

The Kenai Peninsula was heavily glaciated in Pleistocene and Holocene time and the numerous cirques, tarns, moraines, and the characteristic U-shaped valley of the Windy River give evidence to this. An extensive ice cap is still present 25 km east of Red Mountain. Since the retreat of glaciers at Red Mountain, extensive talus slopes have developed at the base of most of the cliffs leaving very little outcrop exposed.

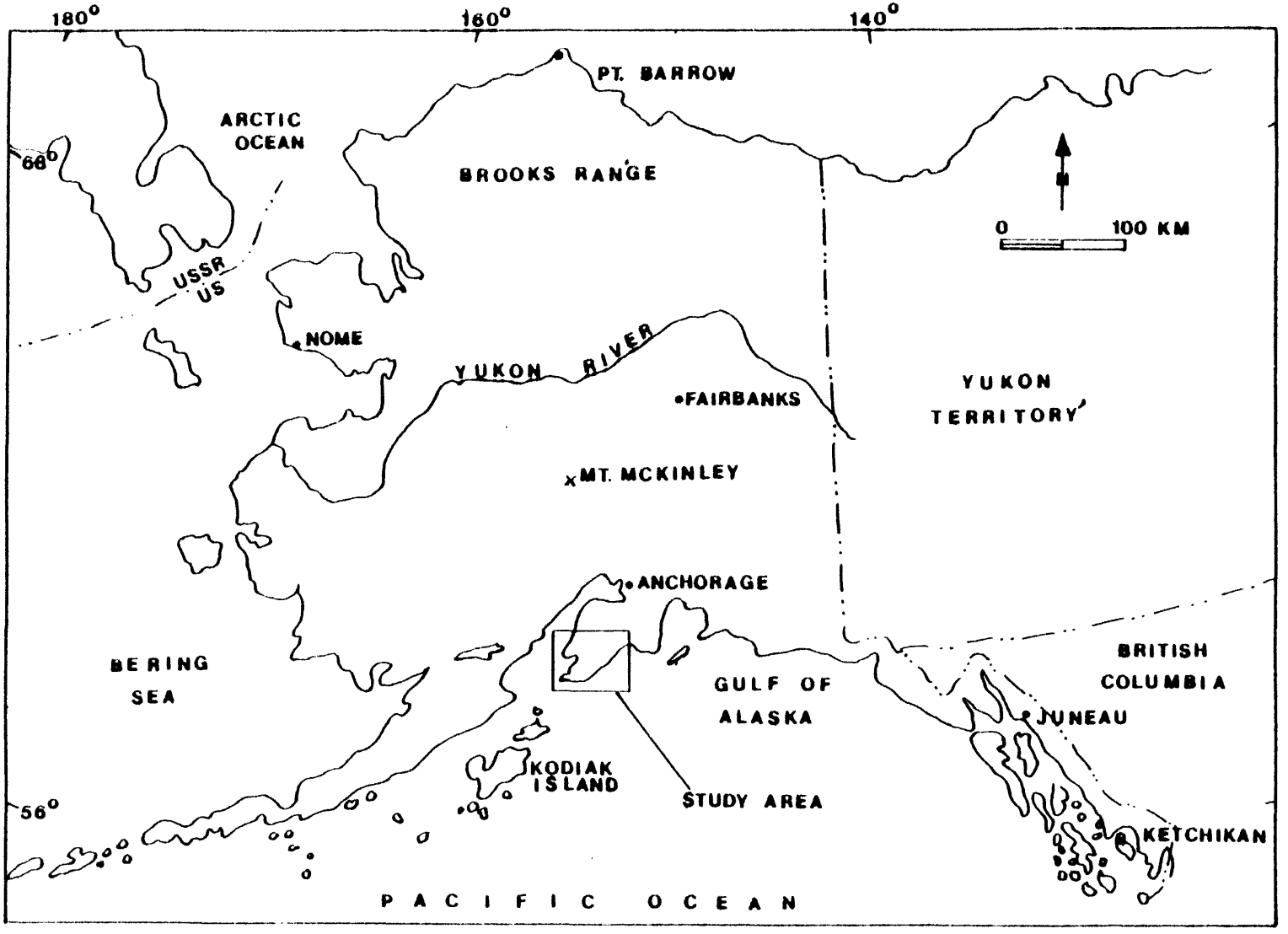

Figure 1.--Index map, Kenai Peninsula, Alaska.

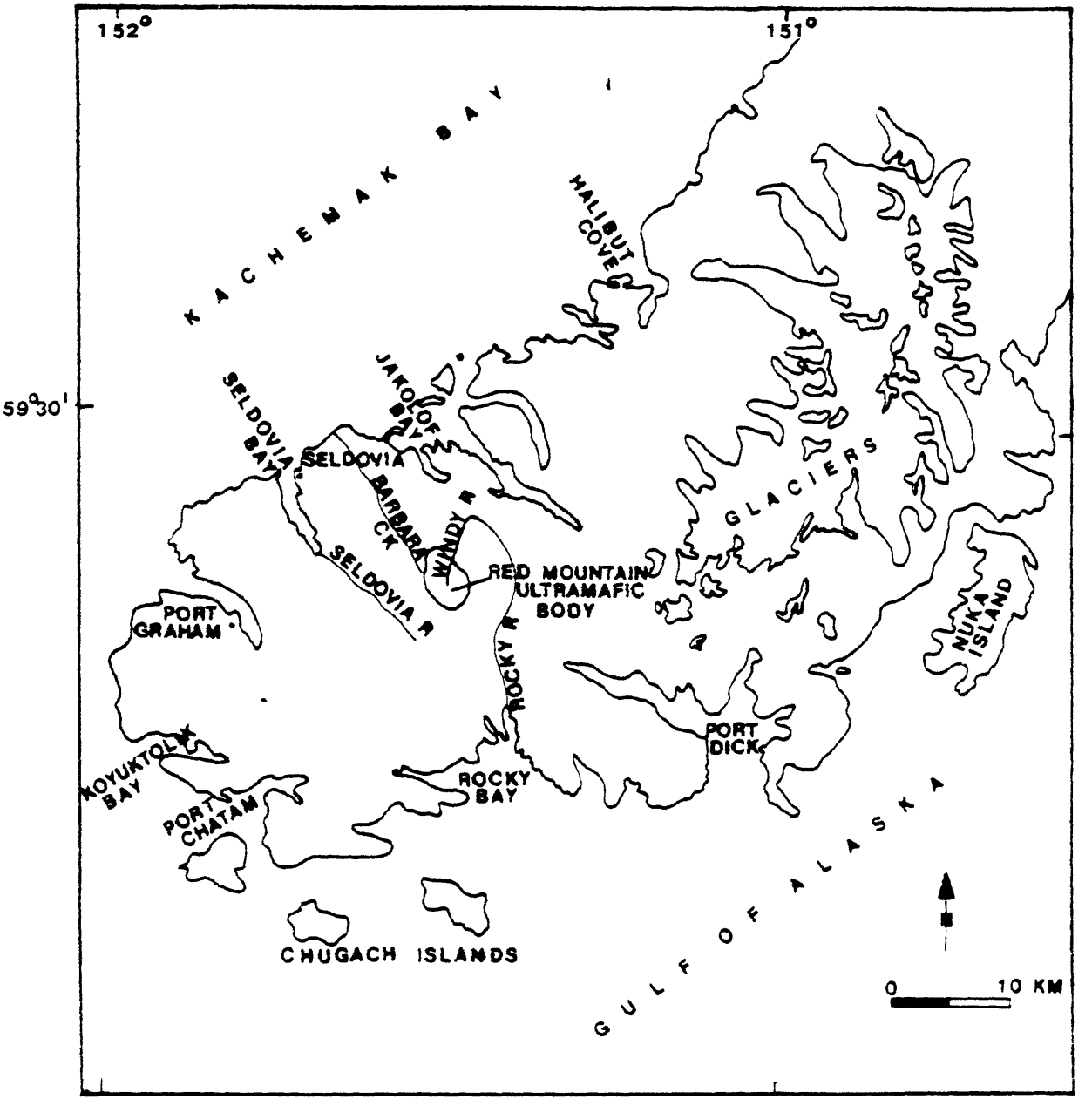

Figure 2.--Map of the southwestern Kenai Peninsula, Alaska.

CHAPTER II

REGIONAL GEOLOGIC SETTING

Nature and Distribution of Major Tectonic Units

Cowan and Boss (1978) have divided the southwestern Kenai Peninsula into four pre-Tertiary tectonic units (fig. 3). Each unit is characterized by a unique rock assemblage and style of deformation and can be correlated with rocks elsewhere in southern Alaska. According to Cowan and Boss (1978), these units suggest that the tectonic history of southwestern Alaska is typified by a long history of seaward accretion by subduction. These four units are discussed below.

An andesitic volcanogenic unit 10 km wide is exposed on the northwestern margin of the Kenai Peninsula (fig. 3), and consists of tuffaceous siltstone, sandstone, and volcanic agglomerate interbedded with black siltstone. The rocks are Late Triassic to Early Jurassic in age and sedimentological evidence suggests that they underwent rapid deposition from nearby sources. Cowan and Boss (1978) correlated the strata with other volcanogenic units exposed throughout southern Alaska. Moore and Connelly (1977) interpreted the volcanogenic rocks as arc and forearc deposits formed in or near a volcanic arc active in Late Triassic and Early Jurassic time.

The Seldovia schist terrane is in a narrow, wedge-shaped bed 2 km wide and 16 km long, extending from Seldovia Point to the northeast shore of Port Graham where it pinches out (fig. 3). The unit consists of quartz-sericite schist, marble, greenschist, and crossite-epidote blueschist immersed in a completely sheared matrix of argillite. Forbes and Lanphere (1973) obtained K-Ar dates for the metamorphism of 190 m.y. (million years) and the schist is correlated by Cowan and Boss (1978) with a narrow belt of metamorphic rocks on Kodiak and Afognak Islands with metamorphic ages of 190-187 m.y. (Carden and

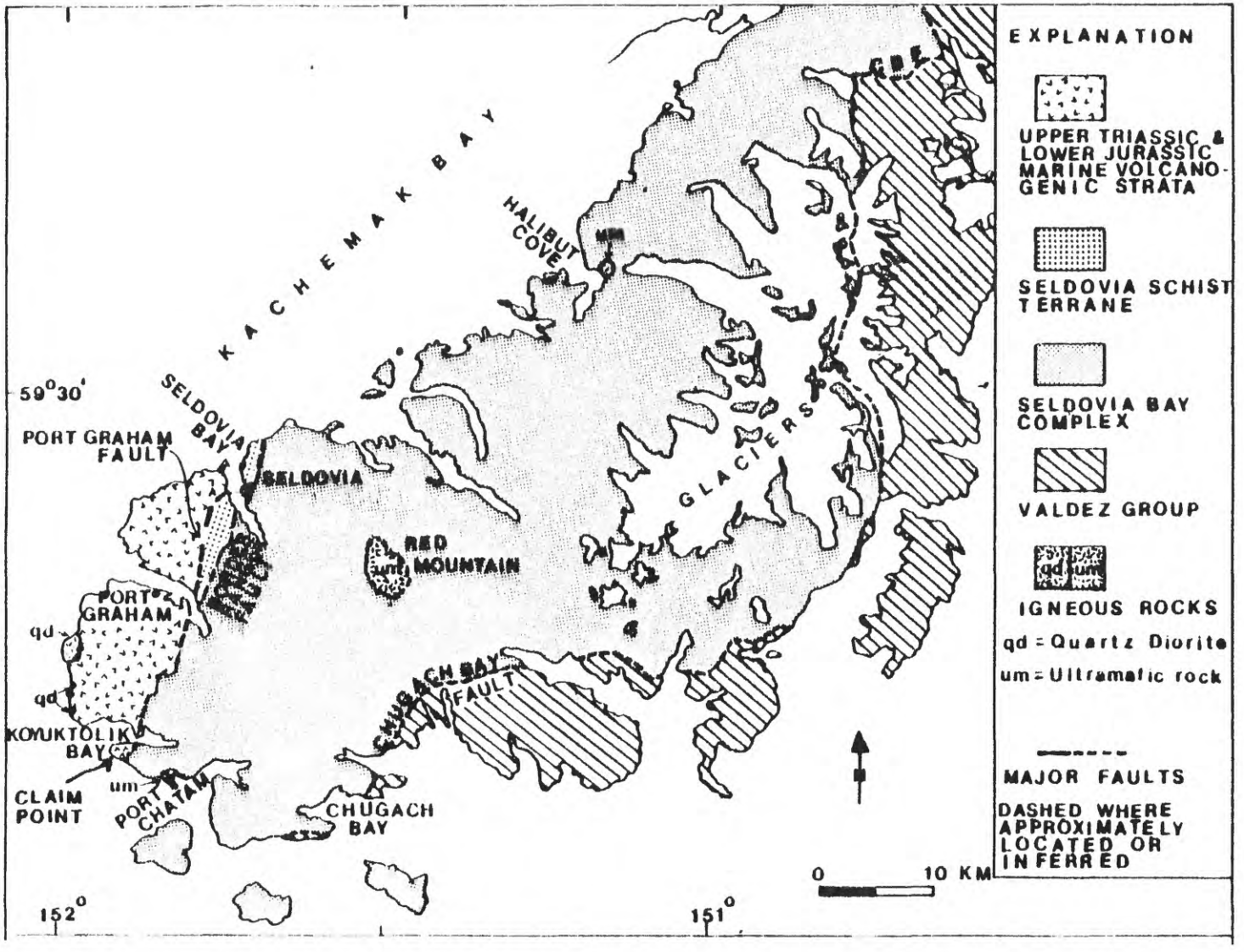

Figure 3.--Geologic map of the southwestern Kenai Peninsula showing pre-Tertiary tectonic units and major faults (modified from Cowan and Boss, 1978).

others, 1977). Cowan and Boss (1978) interpreted the schist terrance as a subduction complex that was emplaced in part during Early Jurassic time simultaneous with blueschist metamorphism.

The Seldovia Bay complex (informal name) forms the core of the southwestern Kenai Peninsula (fig. 3) and is a highly deformed heterogeneous unit of argillite, graywacke, chert, greenstone, tuff, and minor ultramafics, and includes a 2-km-wide terrane of radiolarian chert and pillow lava that extends from Koyuktolik Bay to Halibut Cove. Excluding the ultramafic rocks, the lithologies in the Seldovia Bay complex commonly occur in bedded, sheared, or chaotic sequences. The graywacke frequently shows a weak bedding-plane foliation and minor graded bedding. The attitude of both the bedding and foliation are constant, with the strike to the northeast and dip to the northwest. The studies of Cowan and Boss (1978) show widespread metamorphic pumpellyite and prehnite.

Three ultramafic bodies occur within the Seldovia Bay complex: a small dunite mass at Claim Point; the Red Mountain ultramafic body; and a recently discovered small ultramafic body at the northeast end of Halibut Cove consisting of layered gabbro, pyroxenite, and serpentinite (fig. 3). In all three bodies, contacts with the surrounding country rock are faulted and heavily serpentinized. Correlative ultramafic rocks, greenstones, and gabbros are present on Kodiak Island.

The Seldovia Bay complex is correlated by Connelly and others (1976) on the basis of similar lithology, tectonic style, and metamorphism with the Uyak subduction complex on the northwest coast of Kodiak Island and with the McHugh subduction complex exposed in the Chugach Mountains near Anchorage (Clark, 1972a, 1973).

The Seldovia Bay complex is interpreted by Cowan and Boss (1978) as a Triassic to post-Valanginian subduction complex, and together with the Uyak and McHugh Complexes defines a northeast-trending subduction zone extending for at least 500 km in southwestern Alaska (fig. 4). The ultramafic rocks on Kodiak Island are interpreted as accreted remnants of oceanic crust and mantle (Connelly, 1978; Hill and Gill, 1976; Hill and Brannon, 1976), and I will establish later that the Red Mountain ultramafic body is also part of dismembered oceanic crust. Connelly (1978) stated that the Seldovia Bay complex was emplaced during Late(?) Cretaceous northwest underthrusting beneath lower Mesozoic rocks and during that underthrusting the rocks were broken into varied sizes and suspended in a matrix of chert and argillite with their longest dimension alined subparallel to the cataclastic foliation. During underthrusting the rocks also were metamorphosed on the prehnite-pumpellyite facies.

Connelly (1978) suggested that the Valdez Group exposed to the southeast of the Seldovia Bay complex (fig. 3) may represent a separate phase of Late Cretaceous accretion or that it may be a distinct facies of the Uyak and McHugh Complexes. The Valdez consists of slightly metamorphosed well-bedded turbidite and only local melange. The age is Late Cretaceous on the basis of Maestrictian fossils (J. Decker, oral commun., 1980).

Age of emplacement of the subduction complex is somewhat uncertain. The Uyak Complex contains radiolaria chert ranging from Paleozoic to mid-Early Cretaceous (Valanginian to Aptian); the McHugh Complex contains rocks from late Paleozoic to Late Jurassic age; and some of the chert in the Seldovia Bay complex is Triassic (Cowan and Boss, 1978; Connelly, 1978). Emplacement of the Seldovia Bay complex can thus be determined only to be post-Valanginian, but J. Decker (oral commun., 1980) has dated the subduction of correlative

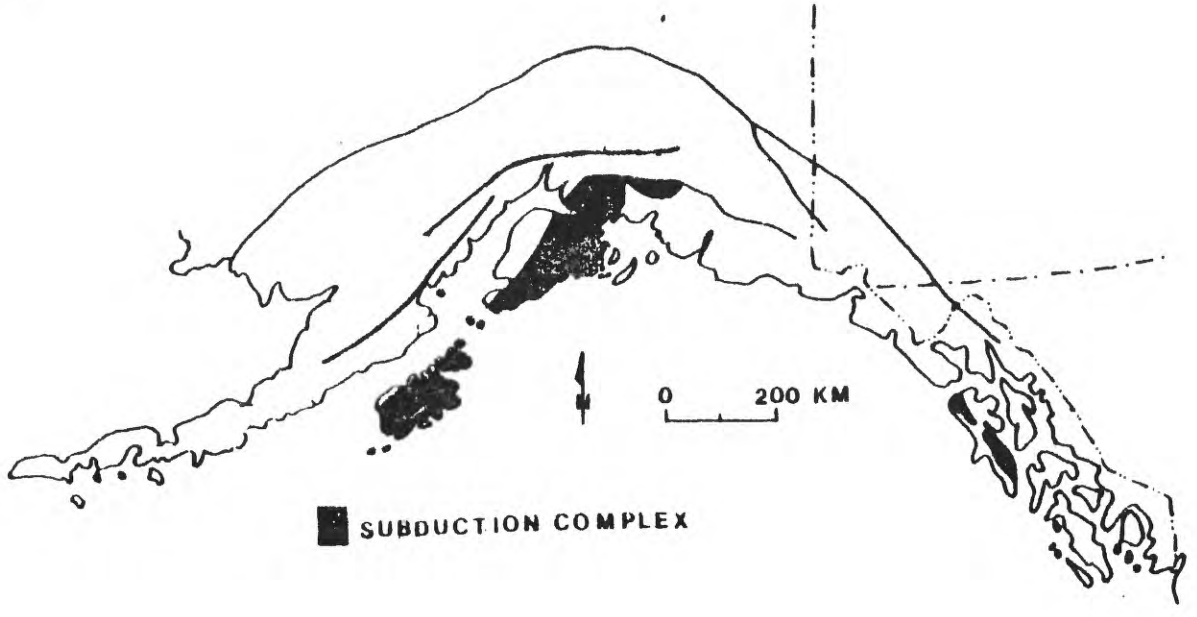

Figure 4.--Distribution of the Seldovia Bay subduction complex and the correlative Uyak-McHugh and Shumagin-Valdez terranes and complex in southeastern Alaska (modified from Moore and Connelly, 1977; complex in southeastern Alaska from J. Decker, oral commun., 1980).

rocks in southeastern Alaska at 100 m.y. by K-Ar dating of metamorphic minerals that probably formed at the time of accretion. The distribution of the rocks emplaced during this episode of subduction is shown in figure 4.

Major Structures

The four tectonic units of the southwestern Kenai Peninsula are separated by major faults that are discontinuously present throughout southern Alaska. These faults are labeled in figure 3.

The Seldovia schist terrane is separated from the Upper Triassic and Lower Jurassic volcanogenic strata by a northeast-trending high-angle fault, herein called the Port Graham fault, which is equivalent to the Shuyak fault on Kodiak Island. The combined Port Graham-Shuyak fault may represent the trace of the early Mesozoic plate boundary along the margin of southwestern Alaska (Connelly, 1978).

The Seldovia Bay complex is juxtaposed against the volcanogenic sequence and the Seldovia schist terrane by the northeast-trending Border Ranges thrust fault. This fault is a major tectonic feature in southern Alaska and can be traced for more than 1,000 km arcuately eastward from Kodiak Island to the St. Elias Mountains (MacKevett and Plafker, 1974). It marks the southern limit of the complex assemblage of Paleozoic and Mesozoic metamorphic rocks and may be the trace of the continental margin at the time of Uyak-McHugh and Shumagin-Valdez accretion.

The major fault juxtaposing the Seldovia Bay complex against the Valdez Group is identified by Cowan and Boss (1978) as the Chugach Bay fault, and they state that it is equivalent to the Eagle River thrust fault near Anchorage and the Uganik thrust on Kodiak Island. The fault typically dips moderately to steeply northwestward although the fault shows a variable attitude around Seldovia. The rocks generally become much more sheared and disrupted

toward the fault. The significance of the fault is unclear due to the uncertainties in the relative ages between the Uyak-McHugh and the Valdez belt. If the units are coeval as Connelly (1978) suggested, then the thrust juxtaposes the more deeply subducted and more highly metamorphosed Uyak-McHugh rocks against the Kodiak-Valdez trench deposits. Connelly (1978) noted that more highly metamorphosed rocks occur along the arcward side of subduction complexes at other convergent margins and that this type of occurrence may be attributed to differential uplift of the subduction complex from continued underplating of deep-sea sediments at the foot of the trench inner wall.

The amount of movement on any one of these faults is unknown but cumulative displacement is probably substantial. Structurally, the volcanogenic unit is on top, underlain by the Seldovia schist terrane and the Seldovia Bay terrane, with the Valdez Group at the base.

CHAPTER III

DESCRIPTION OF THE RED MOUNTAIN ULTRAMAFIC BODY

Field Relations

The Red Mountain ultramafic body is located approximately 13 km southeast of Seldovia on the Kenai Peninsula, Alaska (fig. 1). The body discordantly intrudes country rock mapped by Martin and others (1915) as slate and graywacke with some chert and limestone. Cowan and Boss (1978) described these rocks as commonly bedded, sheared, and forming chaotic sequences. In the vicinity of Red Mountain, the major rock types are a drab, greenish-gray metagraywacke, generally with indistinguishable bedding, and a white to dark-gray, well-bedded, strongly deformed chert unit. The contact of the ultramafic body with the country rock is clearly distinguishable around the entire body because the dunite is a rusty color and supports no vegetation, whereas the country rock supports a luxurious vegetative growth (fig. 5). The contact is a fault, and in a few places where it is actually observable, dips steeply inward from 45° to vertical. The undeflected course of the contact across the hills and valleys also indicates that it must be steep (fig. 5). A serpentinized zone is present in all exposures of the contact and ranges in thickness from 30-50 m in most places, but is nearly 800 m thick near the headwaters of Barbara Creek. The serpentinite zone is better developed in dunite than in pyroxenite, and shows extreme brecciation and slickensides.

No dikes or apophyses of the ultramafic material are found intruding the country rock, and there is no evidence of any thermal metamorphism of the country rock. For these reasons, the body probably intruded the country rock in the solid state. Guild (1942) mapped several small blocks of the country rock within the ultramafic body near the northwestern contact, and these blocks were probably incorporated by the faulting processes. These inclusions

Figure 5.--Red Mountain ultramafic body looking southwest toward Shelikof Strait. Note the well-defined igneous layering and the sharp contacts with the country rock as defined by the contrasting colors of the nonvegetated pluton and the heavily vegetated country rock.

Figure 6.--Wehrlite layer crosscutting chromitite and dunite.

are surrounded by talus, so the exact contact relations with the dunite body are indeterminable.

Form and Structure

The Red Mountain ultramafic body is elliptical in outcrop, 6.5 km long and 3.2 km wide. The body shows well-developed, laterally continuous, primary igneous layering in the dunite, chromitite, and wehrlite. Dunite layers range in thickness from a few millimeters to more than 350 m, and are about 2.3 km long; chromitite layers range in thickness from a few millimeters to 5 m, and are as much as 375 m long; and wehrlite layers range in thicknesses from a few millimeters to 65 m and are as much as 1.5 m long. The three layers may be much more extensive, but are obscured by the heavy talus and alluvial cover. The dunite, chromitite, and wehrlite layers most commonly parallel one another, but occasionally all three lithologies crosscut each other (fig. 6). Contacts between the differing lithologies commonly are sharp (fig. 7), but the dunite-pyroxenite and dunite-chromitite have gradational contacts. Several places within the pluton have been mapped by Guild (1942) as undifferentiated pyroxenite and dunite (pl. 1). In these instances the wehrlite and dunite are interlayered on an extremely fine scale and commonly grade into one another.

The Red Mountain pluton has been folded into a symmetrical synformal structure with the axis plunging toward the southwest (fig. 8 and pl. 2). The dip of the igneous layering is steep to vertical near the contact except in the southwestern part of the body where it is nearly horizontal. Along the axis of the synform, dips are intermediate in the northern part and shallow to near horizontal in the southern part. The strike of the layering parallels the contact along three sides of the body with the strike along the southern margin being almost random. Small-scale folds are common in relatively thin

Figure 7a.--Chromitite layers within dunite. Note the sharp contacts.

Figure 7b.--Wehrlite layers within dunite.

chromitite and wehrlite layers and are present to a minor degree in the garnet pyroxenite bodies. All the folds have axes that are nearly parallel to the axis of the synform, trending south-southwest, and they plunge 20°-58° (fig. 8 and pl. 2). The regional trend of bedding and metamorphic foliation in the surrounding country rocks of the Seldovia Bay terrane is to the northeast.

Joints are abundant in the body, especially around the central amphitheater, and are so well developed that some faces are exposed for an area of more than 100 m^2. The general strike of joints is northwest with a dip of 30°-40° to the northeast. Mineralization is rare along the joint faces but some minor serpentinization is present.

Small-scale faults within the Red Mountain pluton are relatively common and can be clearly identified only when the chromitite or pyroxenite layers have been displaced so little that their original continuity is obvious. Guild (1942) has outlined two periods of faulting: (1) Early faulting--associated with the drag of thin chromite bands. Many of these faults are healed and they antedate final consolidation. These faults commonly show renewed movement, many times in the opposite direction as indicated by "reverse drag." (2) Later faulting--no drag is associated with this episode of faulting and the faults show no healing. Fault zones often show slickensides of serpentine or crushed chromite. Displacements of 0.5-1 m are common, and some are as much as 4-10 m, but no large faults have been found. The fault planes generally coincide with the most pronounced joint planes, striking north-northwest and dipping to the east at low angles.

The Red Mountain pluton is bounded by a major fault. Movement along the fault has probably been substantial, but there is no indication as to the amount of offset or to the age of movement. The fault most commonly contains sheared serpentinite and fragments of brecciated country rock and ultramafic rocks from the pluton.

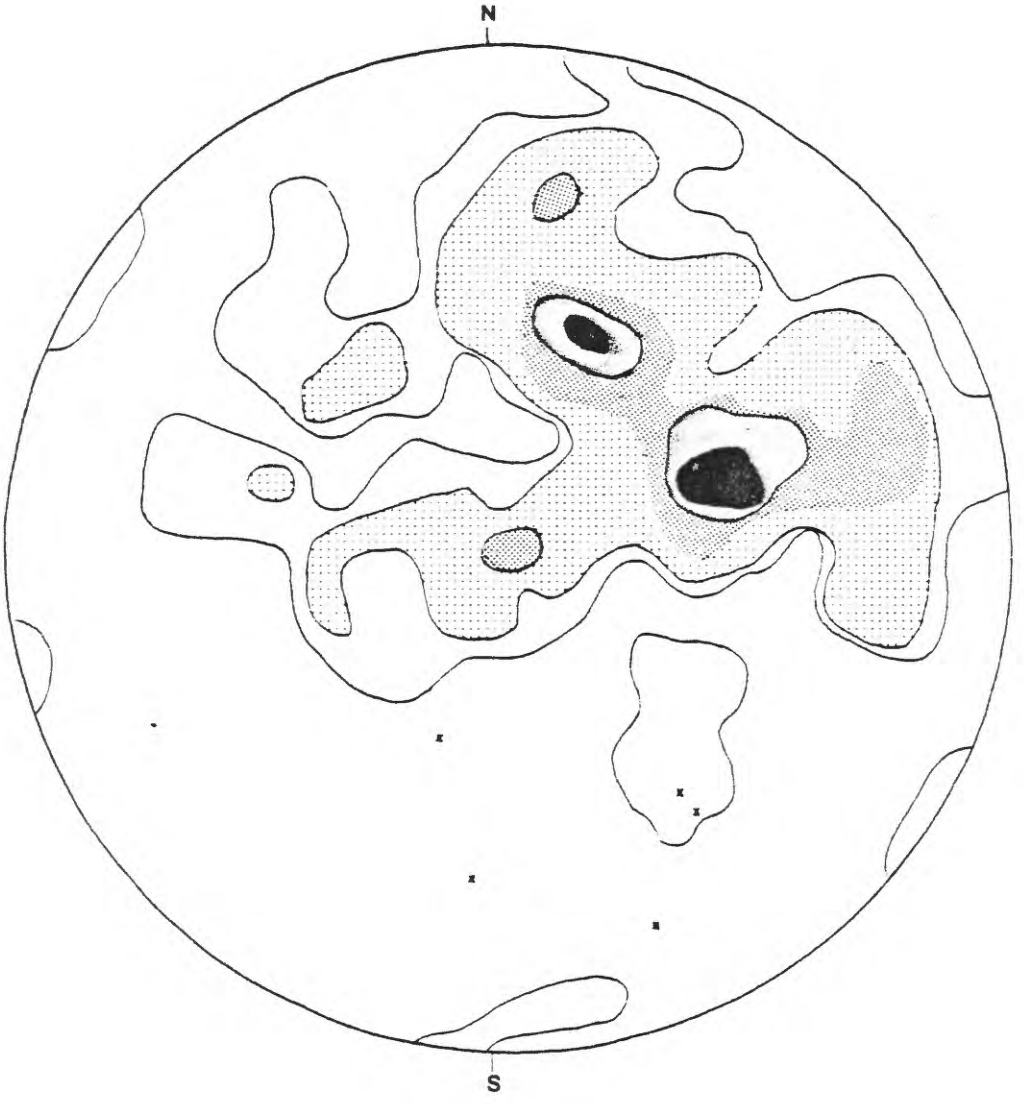

Figure 8.--Stereographic projection of poles to layering within the Red Mountain pluton. Contour intervals: black area, 8 percent; heavy shading, 6 percent; medium shading, 4 percent; light shading, 2 percent; blank outlined areas, 1 percent. Fold aces from chromitite and pyroxenite folds shown by x. Data from Guild (1942) and fieldwork by the author.

Petrology

The rocks exposed in the Red Mountain ultramafic body consist of 90 percent dunite and serpentinite, 10 percent wehrlite, and less than 1 percent garnet clinopyroxenite, clinopyroxenite, chromitite, and minor dike rocks. The classification scheme for naming these rocks is that used by the IUGS (Streckeisen, 1973).

Dunite

In hand specimen fresh dunite is pale green, grading from dark green to black with increasing degrees of serpentinization. The samples show varying degrees of serpentinization, with serpentine occurring both in veins and as pseudomorphic replacements of olivine. With weathering, the dunite develops a rusty, terra-cotta rind, which is a result of the oxidation of the iron in olivine.

Disseminated black metallic chromite is an ubiquitous accessory phase in the dunite, and the grains stand out due to the strong contrast in color and because they weather in relief, yielding a corrugate texture. Chromite comprises 1-4 percent of the rock and is generally subhedral to euhedral with a size range of 1/4-1 1/2 mm in diameter.

Mineralogy: The dunite consists of olivine (Fo_{86}) with ubiquitous accessory chromite. Olivine is commonly altered to serpentine and trace amounts of magnetite, brucite, talc, and calcite. I identified the serpentine tentatively as chrysotile because of its fibrous habit (Heinrich, 1965, p. 309-310; Deer and others, 1975, p. 247-248), but lizardite and (or) antigorite may also be present.

Texture: (1) Primary.--The primary texture in the dunite is typified by a directionless fabric of coarse olivine grains 4-5 mm across, which are anhedral and show irregular interlocking grain boundaries. Chromite occurs in

three modes: disseminated grains 1/4-1/2 mm across (comprising 1-4 percent of the rock), in microscopic layers several millimeters thick (10-90 percent), and as an interstitial phase (<1 percent).

(2) Secondary.--Superimposed on the earlier textures are a series of deformational features which indicate an extremely complex deformational history. The rocks are characterized by bimodal grain sizes, although seriate textures are present. Large, ragged porphyroclasts of olivine 2-3 mm across are surrounded, embayed, and traversed by a fine-grained, recrystallized mosaic of olivine with average grain sizes of 1/10-1/20 mm (fig. 9). This texture has been described in other dunites by Ragan (1963).

The olivine porphyroclasts show severe strain defined by deformational kink bands (Spry, 1969; also called banded olivine by Ragan, 1963) (figs. 9, 10, 12). At least 50 percent of the olivine porphyroclasts show kink bands, and others are probably oriented so as not to show it. The kink bands develop parallel to the (100) plane and have been reported in olivines in other naturally occurring rocks (Ragan, 1963) and in experimentally deformed dunites (Ave'Lallemant and Carter, 1970; Carter and Ave'Lallemant, 1970; Carter, 1976). The kink bands in the Red Mountain olivine show all stages of development from incipiently to sharply defined bands. In the early stages of deformation the olivine grains display diffuse sets of parallel bands of undulatory extinction. With increasing deformation, the bands become sharply defined, showing distinctly different extinction from the adjacent bands.

In a few instances, the dunite shows well-developed schistose fabrics as defined by anhedral, elongate porphyroclasts in an equigranular groundmass (fig. 10). This schistose fabric indicates that recrystallization probably occurred under a directed stress. When chromite layering is present, the schistosity is perpendicular to the layering.

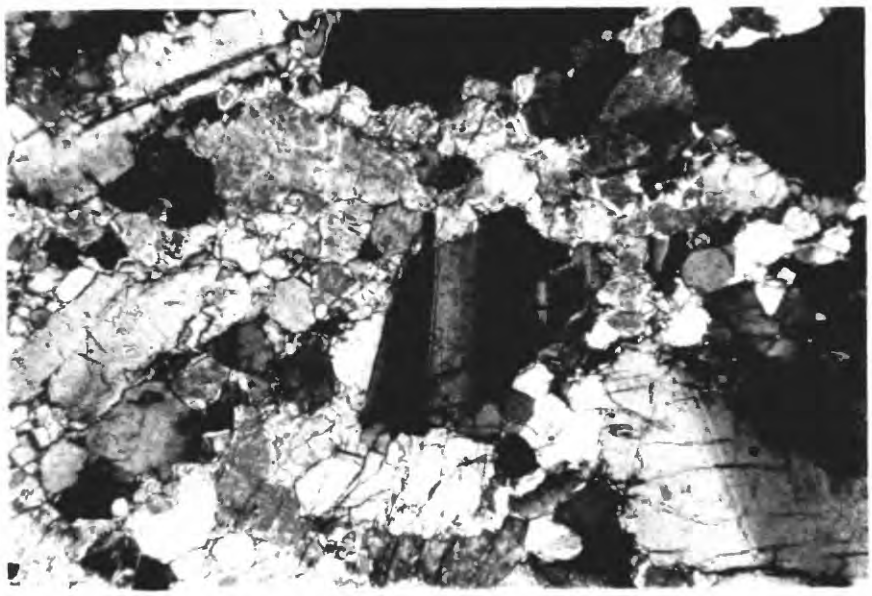

Figure 9.--Photomicrograph showing typical bimodal texture of the dunites. Note that the large porphyroclasts of olivine show well-developed deformational features whereas the groundmass is unstrained. Crossed polars, width of field = 5 mm.

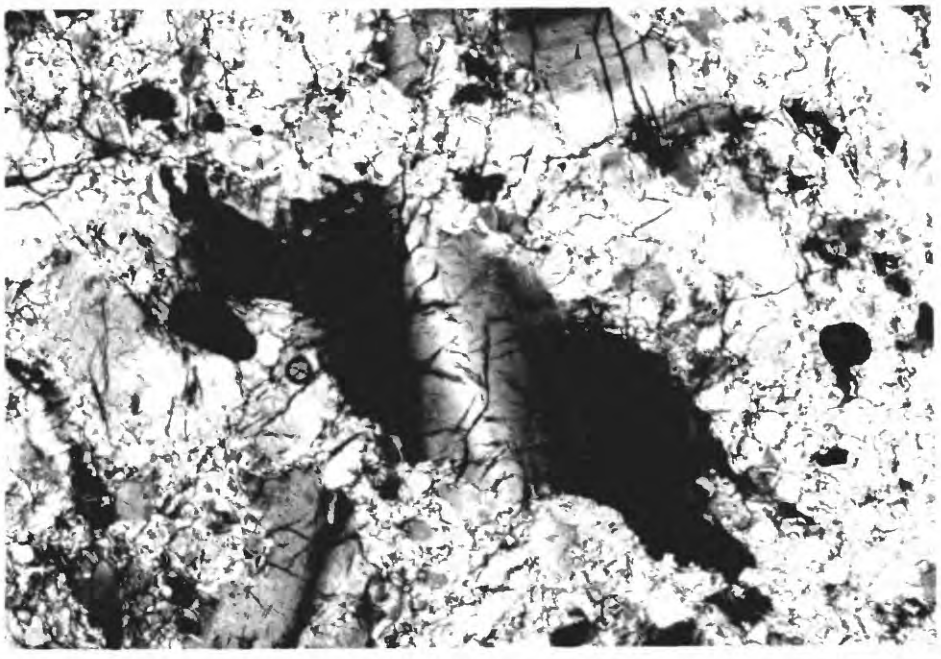

Figure 10.--Photomicrograph of dunite showing a typical elongate porphyroclast which commonly defines the schistosity. Crossed polars, width of field = 4 mm.

The olivine groundmass surrounding the porphyroclasts consists of a mosaic of anhedral, commonly equigranular grains. Straight grain boundaries are present, and in many instances meet at angles of 120°, which minimizes the interfacial energies (fig. 11). Ragan (1969) has discussed this texture in other dunites. In a few instances, the groundmass consists of a fine-grained, optically unresolvable mass, commonly cutting across the porphyroclasts.

Superimposed on these structural fabrics are varying degrees of serpentinization, with weakly serpentinized dunite being rare. Serpentine occurs in veins and as pseudomorphic replacement of olivine. Serpentine veins average 1/10 mm in width and commonly have magnetite cores with associated alteration byproducts of brucite, talc, and calcite. The veins often show small-scale folding, with amplitudes of 2 mm, and a few of the veins are folded with their axes parallel to the foliation. These folded veins are commonly cut by a later generation of undeformed serpentine veins. Many of the olivine and chromite grains show offset where they are cut by serpentine veins due to the volume expansion associated with serpentinization. In many instances, chromite grains are shattered and granulated where they are crossed by a serpentine vein.

Moderately to heavily serpentinized dunite contains vein serpentine and anhedral, strained olivine grains 1/10 mm in diameter floating in a matrix of serpentine. Original grain boundaries are rarely distinguishable.

Wehrlite

In hand specimen the wehrlite is dark green on fresh surfaces, but it commonly weathers to a dark green gray. The rock is crystalline, and a slight schistosity is commonly defined by mineral elongation. Chromite is seldom seen. The wehrlites are fairly resistant to serpentinization and weather in relief compared to the dunites.

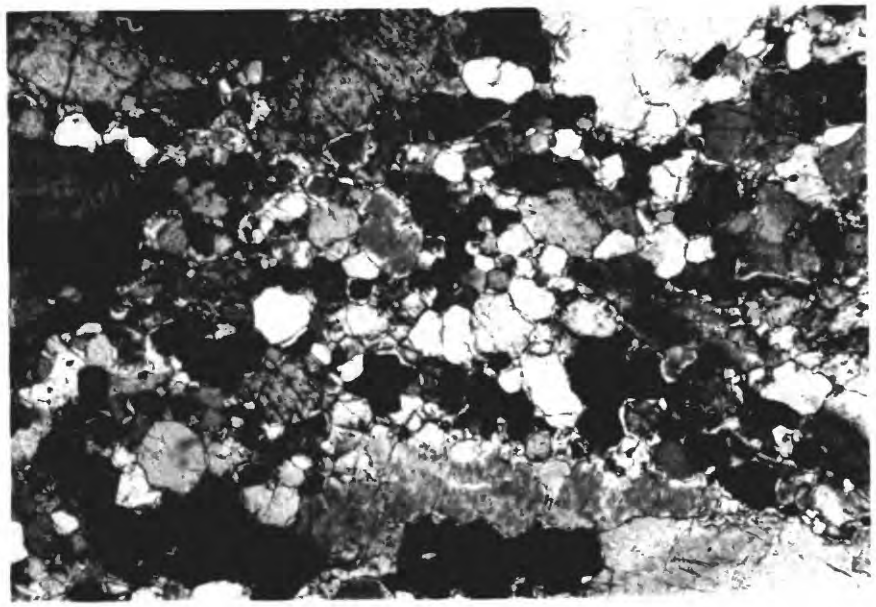

Figure 11.--Photomicrograph of dunite showing a groundmass with a well-developed polygonalized matrix. Many of the straight grain boundaries meet at angles of 120°. Crossed polars, width of field = 5 mm.

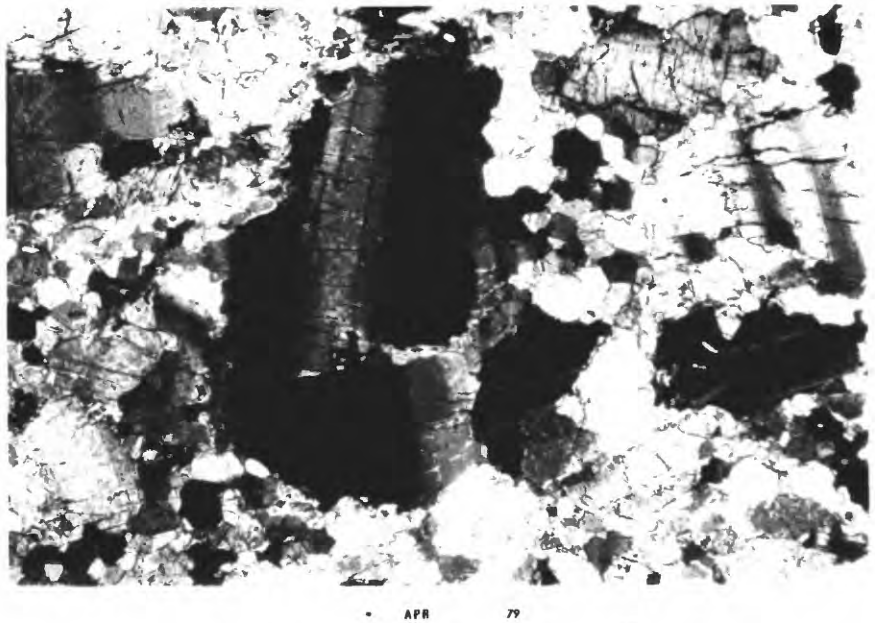

Figure 12.--Photomicrograph of an olivine porphyroclast showing kink bands and intracrystalline recrystallization. Crossed polars, width of field = 4 mm.

Mineralogy: The wehrlite consists of diopside, olivine (Fo_{83}-Fo_{86}), and minor amounts of chromite. Diopside shows well-developed cleavage and commonly developed parting along (100). No exsolution features are present. Twins are common and occur as broad lamellae. Optic angles of diopside measured on the universal stage range from 55-56+. Olivine is unzoned and commonly shows good development of one direction of cleavage. Alteration products include rare serpentine, amphibole, and chlorite.

Texture: (1) Primary.--The primary texture of the wehrlite is typified by interlocking grains of olivine and diopside with diameters of 2-4 mm. Olivine is anhedral to subhedral, whereas diopside is subhedral to euhedral. Chromite (1-2 percent) is present as disseminated euhedral grains 1/8-1/4 mm across. The texture is hypidiomorphic granular and chromite commonly shows an interstitial habit.

(2) Secondary.--Superimposed on the primary textures is a sequence of deformational features similar to those in the dunites. The most common texture is microporphyroclastic to seriate (fig. 13). Porphyroclasts of subhedral to euhedral diopside 2 mm across and anhedral, embayed, and ragged olivine 1 to 1 1/2 mm across are present in a fine-grained matrix (fig. 14). The average size of grains in the matrix is 1/10-1/4 mm across, but the matrix is commonly so fine grained as to be optically unresolvable.

In all the wehrlites studied, both the olivine and diopside grains show evidence of severe strain, although the olivine more commonly shows deformational features. Olivine typically developed kink bands similar to those observed in the dunite, and it shows extensive recrystallization. Diopside grains may be bent, and commonly show undulatory extinction; evidence of recrystallization within diopside grains, however, is rare. For this reason, I assumed that all the matrix material is recrystallized olivine; the

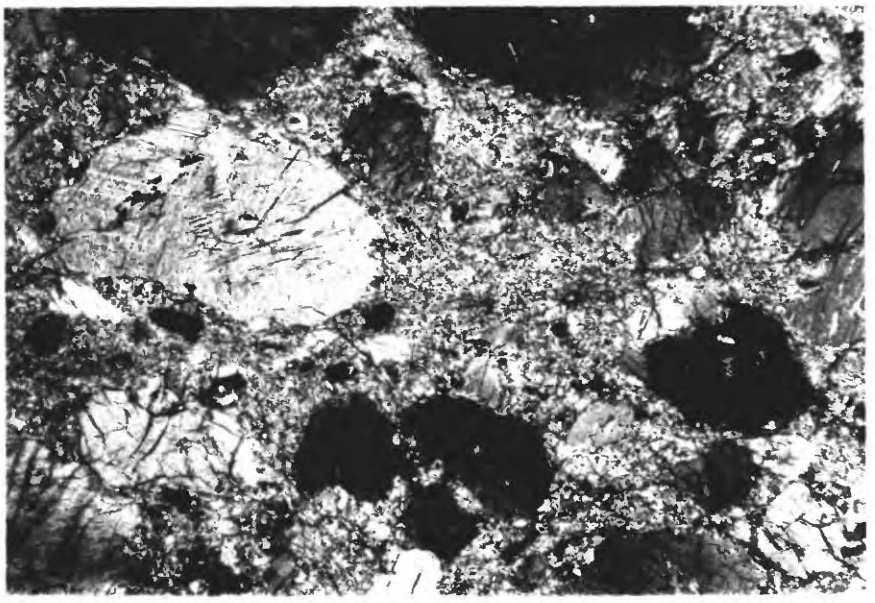

Figure 13.--Photomicrograph of wehrlite showing well-developed microporphyroclastic texture. The dark grain in the upper center of the photograph was probably once a continuous olivine grain which has undergone recrystallization and possible rotation. Crossed polars, width of field = 5 mm.

Figure 14.--Photomicrograph of wehrlite showing strong embayment of an olivine porphyroclast. Crossed polars, width of field = 5 mm.

amount of olivine porphyroclasts and matrix is then the original olivine content of the rock. Assuming that this content is a maximum value, the maximum olivine content ranges from 42-69 percent. If there is substantial diopside in the groundmass, then the rock would be classified as olivine clinopyroxenite. The modal composition of the rocks probably overlaps the wehrlite/olivine clinopyroxenite boundary.

Several individual thin sections show well-developed transitions from a primary, hypidiomorphic granular texture to a microporphyritic texture (fig. 15A-C). This transition is first indicated by the recrystallization and rarer polygonalization of olivine grains, which occurs preferentially along the grain boundaries between olivine and diopside. Within a few millimeters the recrystallized areas become progressively finer grained until they sometimes become optically unresolvable. Several millimeters away, further recrystallization produces a microporphyritic texture.

Recrystallization of olivine in the wehrlite results in a very fine grained rock, whereas recrystallization of olivine in the dunites produces a much coarser grained rock. This may be a function of the heterogeneous mineralogy. In the dunite, much of the recrystallization begins within individual olivine grains, whereas in the wehrlite most of the recrystallization is initiated at grain boundaries, which seems to facilitate further recrystallization.

The wehrlite also shows some minor evidence of cataclasis. In a few of the thin sections, sheared chromite grains define a schistosity as do sheared, elongate olivine porphyroclasts (fig. 16). These cataclastic zones are generally only a few millimeters wide and of limited occurrence.

Serpentinization of the wehrlite is not common, and is generally restricted to veins. Olivine, diopside, and chromite show well-developed offset where crossed by a serpentine vein due to the volume expansion

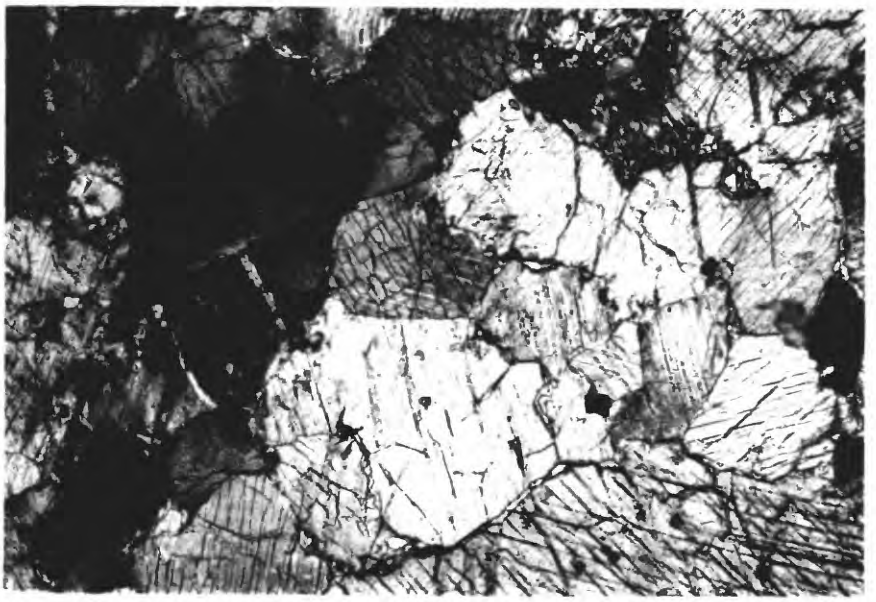

Figure 15a.--Photomicrograph showing relict primary texture of wehrlite.

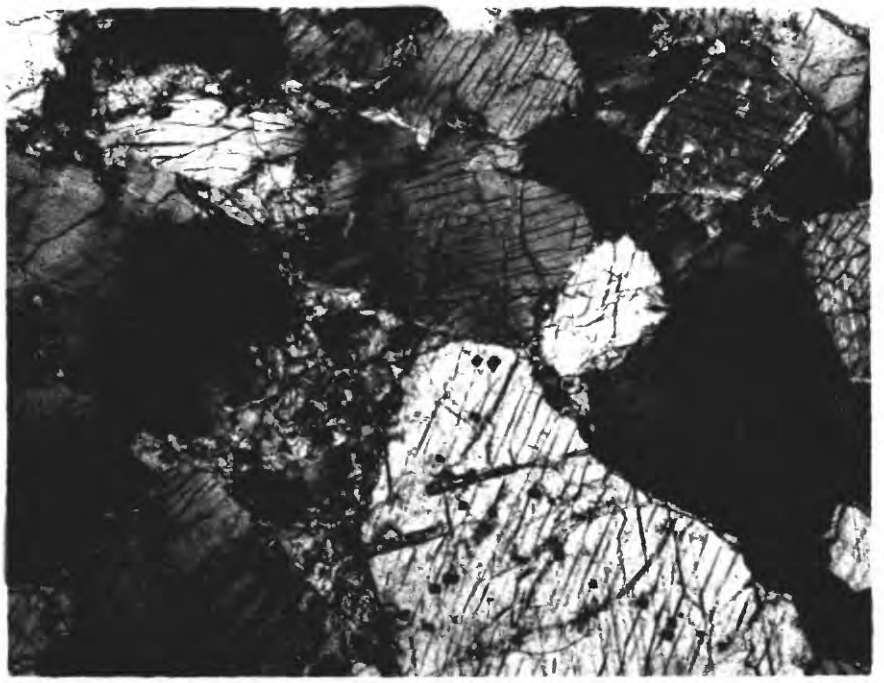

Figure 15b.--Photomicrograph taken a few millimeters from figure 15a showing incipient recrystallization of olivine along olivine-diopside grain boundaries. Crossed polars, width of field = 5 mm.

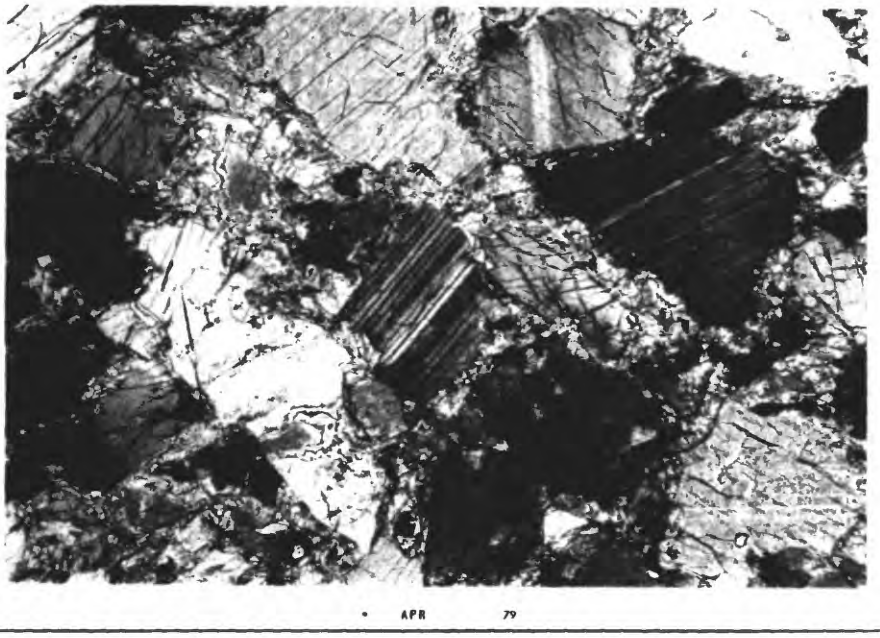

Figure 15c. Photomicrograph taken a few millimeters from figure 15b showing further recrystallization of the wehrlite, approaching a microporphyroclastic texture. Crossed polars, width of field = 5 mm.

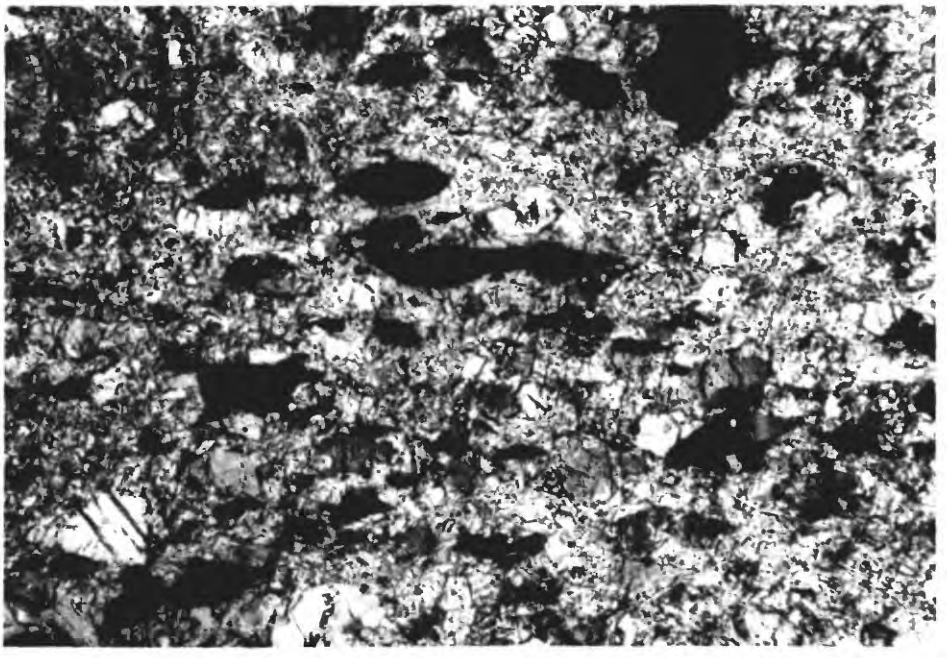

Figure 16.--Photomicrograph of wehrlite showing a strongly recrystallized groundmass and elongation of chromite grains (black grains). Crossed polars, width of field = 5 mm.

associated with serpentinization. Magnetite is a commonly associated byproduct and occurs in the cores of the serpentine veins. Chlorite and amphibole are present in minor amounts as alteration products of diopside.

Clinopyroxenite

The clinopyroxenite is similar in outcrop to the wehrlite. The clinopyroxenites are dark green on fresh surfaces, and are crystalline and equigranular. No schistosity is evident. Alteration to serpentine is rare and chromite is not detectable.

Mineralogy: The clinopyroxenite consists of 90-93 percent diopside, 7-10 percent olivine (Fo_{84}), minor chromite, and trace amounts of chlorite and serpentine. Diopside shows well-developed cleavage and parting along (100). Optic angles of diopside are 55-57°(+).

Texture: (1) Primary.--The clinopyroxenites are characterized by interlocking grains of diopside and olivine averaging 1 1/2 to 2 mm in diameter, but some grains are as much as 3 mm in diameter. Textures are idiomorphic granular (fig. 17).

(2) Secondary.--Almost no deformational features are present in the clinopyroxenite. Two of the four thin sections studied showed no recrystallization or cataclastic features. The other two slides show rare development of the deformational textures observed in the wehrlite. The clinopyroxenite presumably underwent the same deformational history as the dunite and wehrlite and yet shows few of the same deformational features. This deformation is most likely a function of the homogeneity of mineralogy and the structure of diopside. I have established earlier in this report that olivine-diopside grain boundaries are more susceptible to the deformation than are homogeneous grain boundaries.

Figure 17.--Photomicrograph of clinopyroxenite showing an idiomorphic granular texture. Crossed polars, width of field = 4 mm.

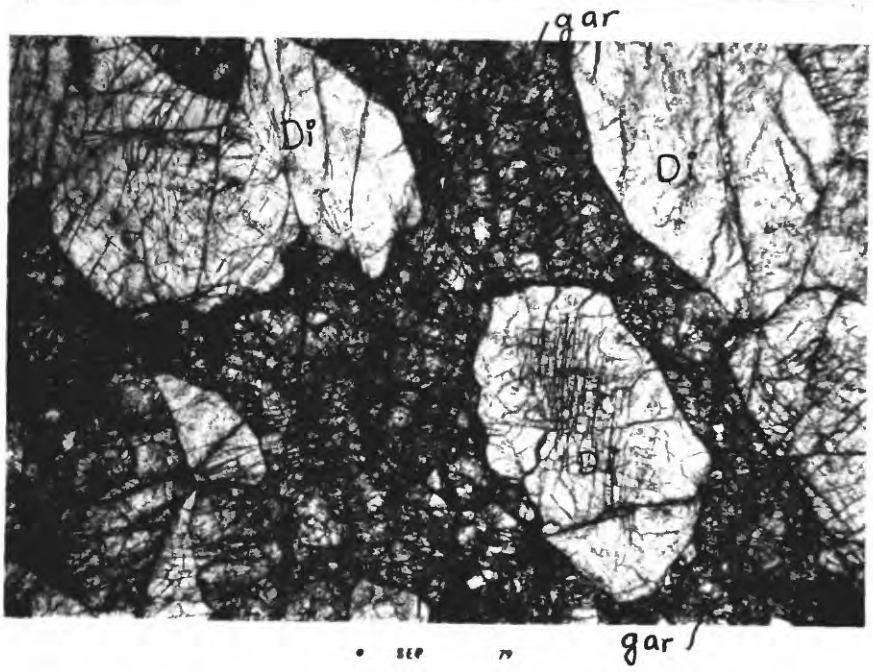

Figure 18.--Photomicrograph of garnet-rich garnet clinopyroxenite showing strong deformation and shearing of the garnet. Plane polarized light, width of field = 5 mm. gar = garnet; di = diopside.

Garnet clinopyroxenite

The garnet clinopyroxenite occurs in six irregular and lens-shaped masses along the north margin of the Red Mountain pluton. They range in size from 15 to 90 m across. The bodies are commonly surrounded by dunite talus with a narrow serpentinite zone between the two. Variation in the modal ratio of garnet to diopside defines a coarse foliation within the lenses. At megoscopic scale, layers 5 cm to 1 m thick of garnet-rich rocks (65 percent garnet) alternate with garnet-poor (35 percent garnet) rocks. The garnet-rich rocks are dark pink, and crystals of dark-green diopside 5 mm long are present in a matrix of nonvitreous garnet. The garnet-poor rocks contain anhedral masses of garnet 5-10 mm long in a matrix of coarse-grained, idiomorphic diopside crystals. On a small scale, foliation is defined by layers of diopside a few millimeters thick in which the diopside shows a strong elongation.

Mineralogy: The mineralogy of the garnet pyroxenite bodies is dominated by garnet and diopside, but ilmenite is an ubiquitous accessory mineral. Diopside grains average 1 1/2 to 2 mm in length but commonly are as much as 5 mm long. One direction of cleavage is present but the (100) parting was not observed in the wehrlite and clinopyroxenite. Amphibole and sphene occur in minor amounts.

Texture: The fabric of the garnet pyroxenite is ambiguous and may be interpreted as either igneous or metamorphic. In the garnet-rich rocks, garnet poikilitically encloses elongate and strongly schistose diopside grains. In the garnet-poor rocks, garnet occurs as a xenomorphic interstitial phase. The garnet pyroxenite rocks may have crystallized directly from a melt and have since undergone metamorphism.

The diopside in the rocks shows strong undulatory extinction, right-angle bends of cleavage traces and twins, deformation lamellae, and broken crystals. Amphibole is common, either as a pseudomorphic replacement of diopside, or along diopside-garnet boundaries. No exsolution features are visible. The garnet is extensively sheared and granulated (fig. 18) and is cut by a network of alteration veins, composed of amphibole or rarer chlorite.

Chromitite

In hand specimen chromitite is metallic black and contains 10-40 percent interstitial olivine, which has weathered to a rusty color. The chromite weathers in relief, giving most of the chromitites a corrugated texture.

Mineralogy: The chromitite consists of chromite and olivine (Fo_{92}). Serpentine is common as an alteration product of olivine.

Texture: (1) Primary.--The primary texture of the chromitite is typified by euhedral grains of chromite 1-2 mm across and interstitial anhedral olivine. The texture is orthocumulate, and the chromitite is the only rock at Red Mountain that give clear evidence of cumulate origin.

(2) Secondary.--The only deformational feature observed in the chromitite is the recrystallization of olivine into a very fine grained mass, which is sometimes optically unresolvable and similar to the recrystallized olivine in the wehrlite.

Dikes

Dikes are rare in the area studied. As discussed by Guild (1942), the dikes are usually less than 2 cm thick, but in a few places they are as much as 1 m thick. They generally cut the primary layering. The mineralogy includes pure olivine, pyroxene, and hornblende dikes as well as dikes made up of mixtures of these minerals. At Red Mountain, dikelets containing major

anorthite with accessory hornblende, olivine, pyroxene, garnet, and spinel are prominent because anorthite is the only light-colored silicate found within the intrusive.

Chemistry

Major-element chemistry

Major-element chemical analyses were performed by the U.S. Geological Survey for the dunite, wehrlite, and garnet clinopyroxenite by the techniques discussed by Peck (1964) (Appendix, tables 1, 2, and 3). These analyses were normalized to 100 percent after subtracting water in order to compare the analyses to those of other ultramafic rocks. Assuming serpentinization is an isochemical process except for the addition of water, this recalculation also corrects for any serpentinization. Because oxidation of iron is a result of serpentinization, the iron is recalculated as FeO (FeO*). Although some Fe_2O_3 may be present in chromite, this recalculation is justified because of the minor abundance of chromite (1-4 percent). After completing these recalculations, the MgO/MgO+FeO*+MnO were determined for the dunite (fig. 19). The median value is 0.86, with a range of 0.77-0.89. The dunite and wehrlite show extreme depletion in the alkali elements, with Na_2O+K_2O consistently less than 0.05 percent of the whole rock. Al_2O_3 is also low, averaging less than 1-2 percent of the whole rock. The alkali elements in the garnet clinopyroxenite average less than 0.5 percent, but in contrast to the dunite and wehrlite, Al_2O_3 ranges from 6.62 to 8.29 percent. SiO_2 is also low, ranging from 39-41 percent. The composition of the garnet clinopyroxenite most closely resembles the average mellilite nephelinite of Nockhold (1954) and that of a New Zealand olivine nephelinite of Benson (1942). Figure 20 shows the extremely restricted compositional range for the Red Mountain rocks.

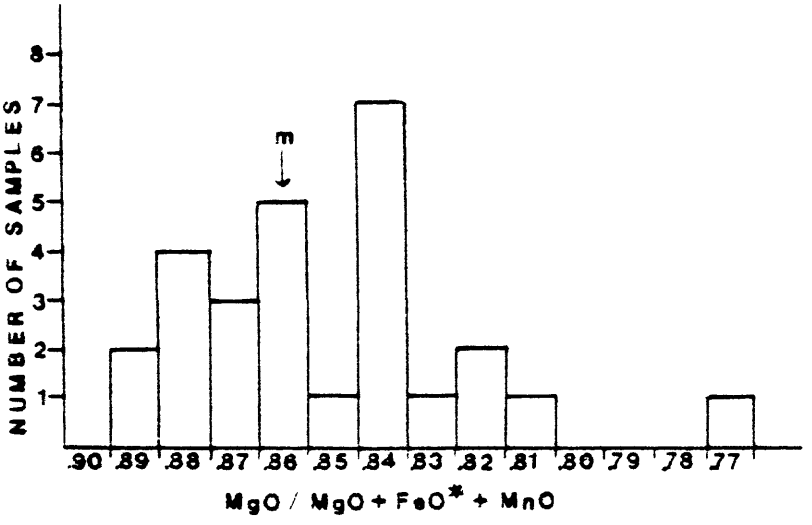

Figure 19.--Histogram showing MgO/MgO+FeO*+MnO in dunites from Red Mountain. FeO* = total iron as FeO. m = median.

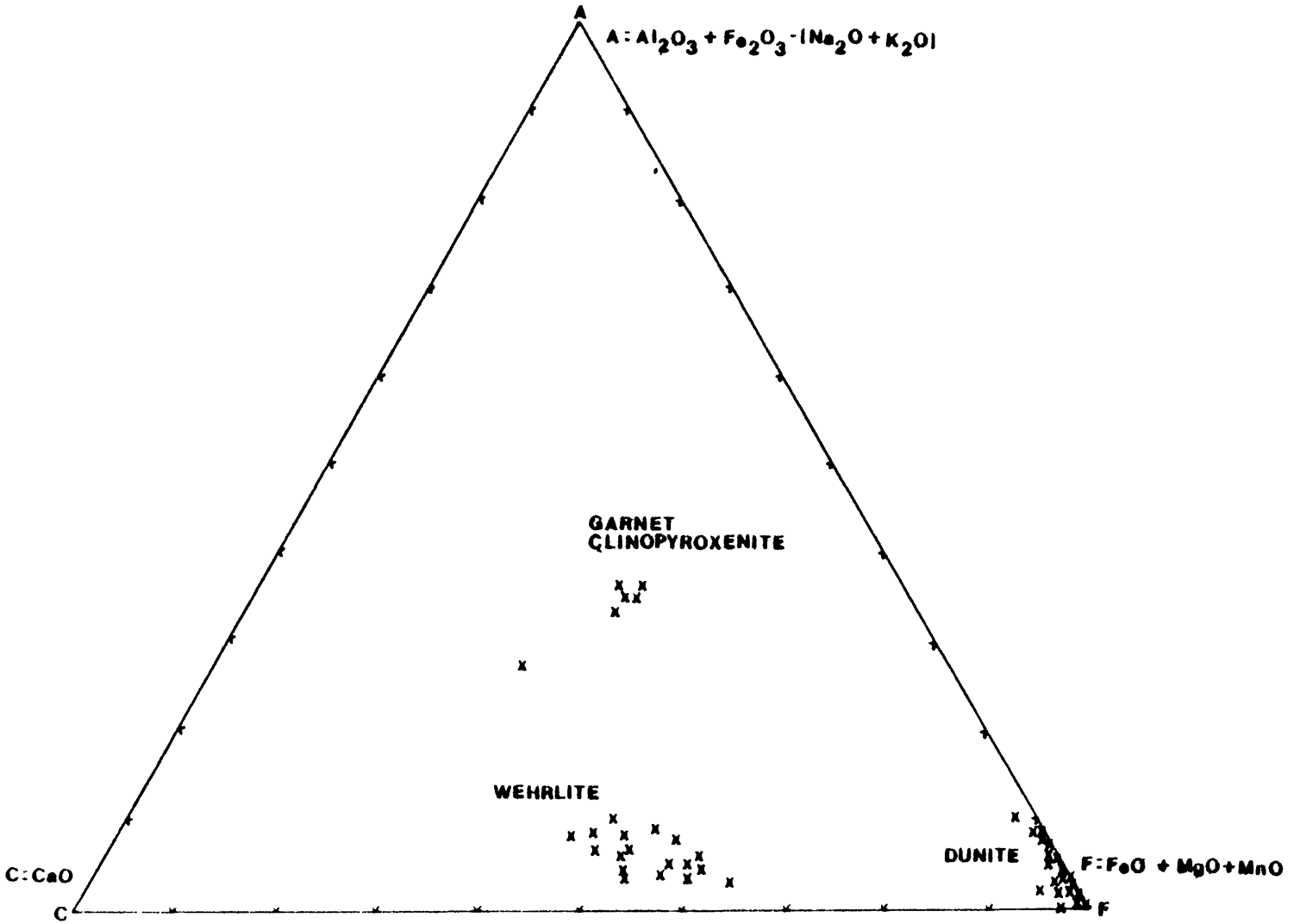

Figure 20.--ACF diagram showing the composition of the dunite, wehrlite, and garnet pyroxenite from Red Mountain, Alaska.

Mineral Chemistry

Dunite: As the dunite is dominantly monominerallic, the MgO/MgO+FeO*+MnO should reflect the forsterite content of the olivine. This implies a median forsterite content of Fo_{86}, which is the same as that determined by optical methods. Samples showing low water content (<1 percent) should yield even more accurate composition data because they have undergone little alteration. These samples range from Fo_{77} to Fo_{88}, with a median value of Fo_{87}. Several olivine grains in a single dunite sample were analyzed by the Applied Research Laboratory (ARL) microprobe for major elements (Appendix, table 4), and yielded an average forsterite content of Fo_{84}, assuming all iron is present as Fe^{2+}. No compositional zoning was detected. Olivine in a sample with 90 percent chromite yielded a forsterite content of Fo_{92}, assuming all iron is present as Fe^{2+}.

I also probed chromite grains in both the dunite and chromitite (Appendix, table 5). The chromite that occurs in the chromitite is more MgO- and Cr_2O_3-rich than that in the dunite and is correspondingly lower in FeO and Al_2O_3. The olivine in the chromitite also has a higher MgO content than in the dunite. Wet chemical analyses by Guild (1942) indicated that the chromite averages 58 percent Cr_2O_3 and shows Cr-Fe ratios of 2.6:1 to 3.5:1.

Wehrlite: Both olivine and diopside were analyzed by the microprobe, and the results of this work and end-member calculations for the pyroxenes are shown in the Appendix in table 6. No chromite grains were analyzed. Several olivine grains in sample 341X were probed, yielding a forsterite content of Fo_{84}, assuming all the iron is present as Fe^{2+}. This value is slightly higher than that for the olivine studied in the dunite. No compositional zoning was detected.

Diopside grains from two different samples were analyzed. Sample 341X is a typical wehrlite and sample 377 is an almost monominerallic clinopyroxenite with a few percent olivine. Both samples yielded similar compositions and were unique in that no detectable Al_2O_3 was present in either sample. Several different grains were probed for Al_2O_3 to verify this observation. The pyroxenes are also marked by an unusually high CaO content, with Ca-Ca+Mg atomic ratios ranging from 0.57 to 0.59. The pyroxene compositions can be represented by the three end members, enstatite, ferrosilite, and wollastonite, and their composition is dominantly a mixture of enstatite and wollastonite (Appendix, table 6).

Garnet Clinopyroxenite: Diopside grains from specimens 031A and 032 were analyzed by the microprobe and the data are presented in the Appendix in table 6 with wet chemical analyses as determined by Forbes and Swainbank (1974). The pyroxenes show a fairly restricted compositional range and are marked by a high CaO content and an unusually high Cr_2O_3 content.

Tschermaks molecule ($CaAlAl_2SiO_6$) ranges from 14.5 to 18 percent in the pyroxenes from the garnet pyroxenites in contrast to the pyroxenes from the wehrlites and clinopyroxenites which show no Tschermaks molecule (Appendix, table 6). The pyroxenes from the garnet-bearing rocks also show lower SiO_2 and MgO and higher total FeO* in comparison to the pyroxenes from the wehrlites and clinopyroxenites. Both pyroxenes are unusual in their low alkali content, but the pyroxenes from the garnet-bearing rocks are especially unusual when compared to other pyroxenes from garnet-bearing rocks (see Forbes and Swainbank, 1974). The pyroxenes from Red Mountain are not only unusual in their high Tschermaks molecule but they are also extremely low in jadeite content.

Compositional determinations of garnet by the microprobe and from mineral separates by Forbes and Swainbank (1974) are given in the Appendix in table 7. End-member calculations are also presented based on six oxygens from Forbes and Swainbank (1974). End members were not determinable for the microprobe analyses because Fe^{2+}/Fe^{3+} are unknown. Forbes and Swainbank (1974) plotted the garnet compositions on an end-member diagram with several other garnets from ultramafic rocks whose composition is given in the literature. They found that the garnets which are most similar to the Red Mountain garnets are those from kyanite-eclogite fragments associated with inclusions from a kimberlite pipe in Yakutia. These garnets have a low alkali content similar to that of Red Mountain rocks, averaging less than 0.1 percent Na_2O+K_2O. Forbes and Swainbank (1974) also pointed out that the composition of the Red Mountain garnet samples is an example of solid-solution composition in an interval that was formerly believed to be an immiscibility gap in the garnet series.

Trace-element chemistry

Trace-element chemistry was obtained from the U.S. Geological Survey on the dunite and wehrlite by six-step 30-element emission spectrometry (Grimes and Marranzino, 1968) (Appendix, tables 8 and 9), by atomic absorption for chromium and nickel (Appendix, table 10), and by fire assay for platinum, palladium, rhodium, ruthenium, and iridium (Appendix, tables 11 and 12). Results of this work show that the dunite and wehrlite are characterized by few detectable trace elements. Figures 21 and 22 show the range in abundances of the detectable trace elements and median values for each element. Most of these trace elements show concentrations similar to those given by Wyllie (1967) for the "average" ultramafic rock. For the dunites, chromium, nickel, and vanadium are substantially higher than the average value of Wyllie (1967),

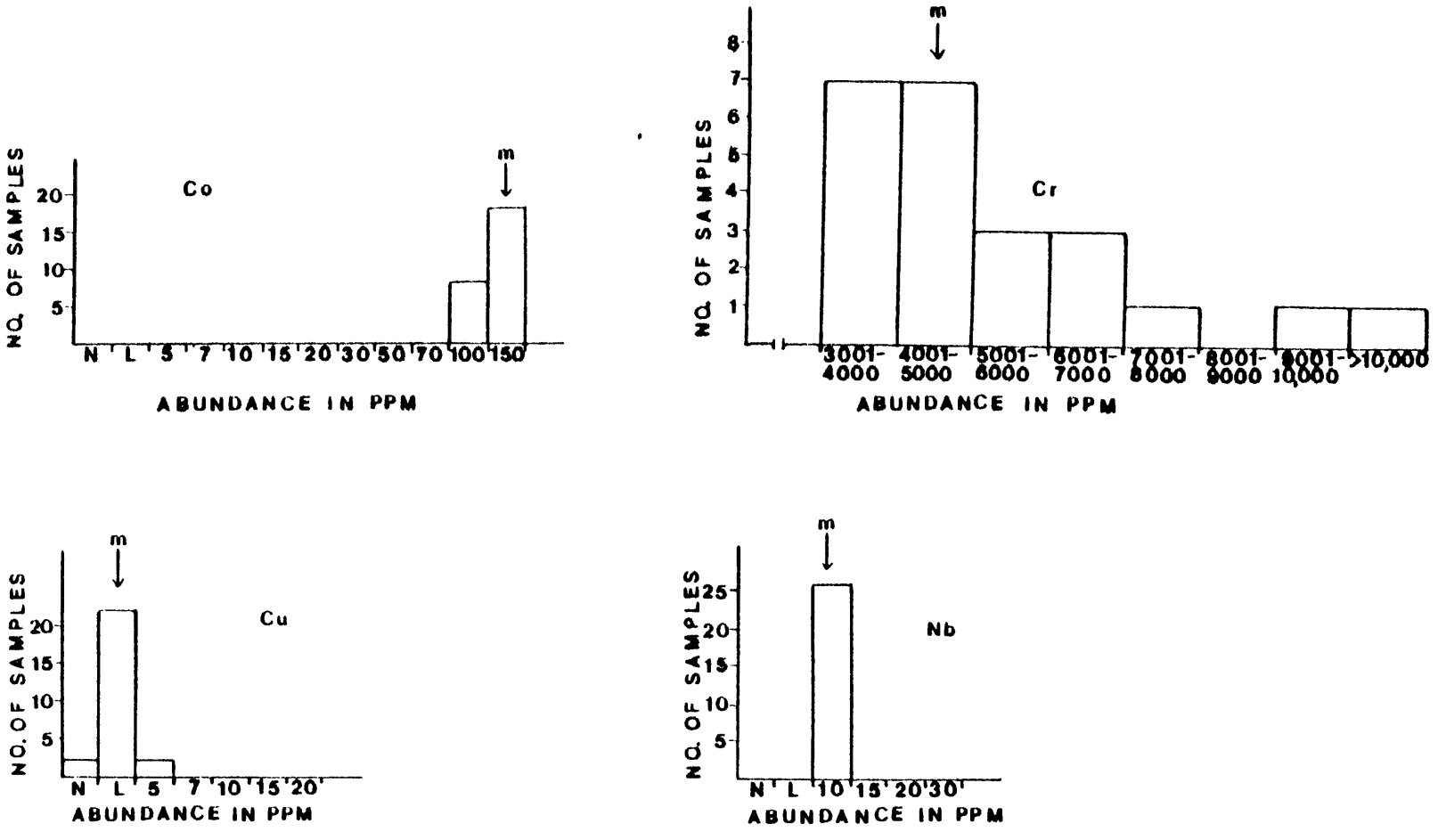

Figure 21.--Histogram of detectable trace elements in dunite, Red Mountain ultramafic body, Alaska. Analyses by emission spectrographic methods, except for chromium and nickel which were analyzed by atomic absorption (analysts K. J. Curry and Z. C. Stephenson). m = median.

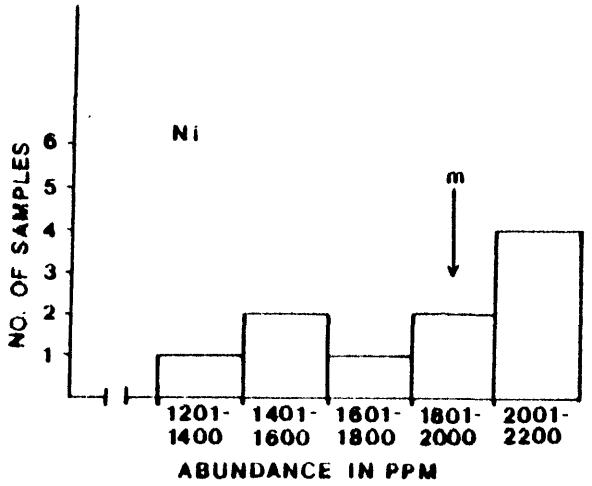

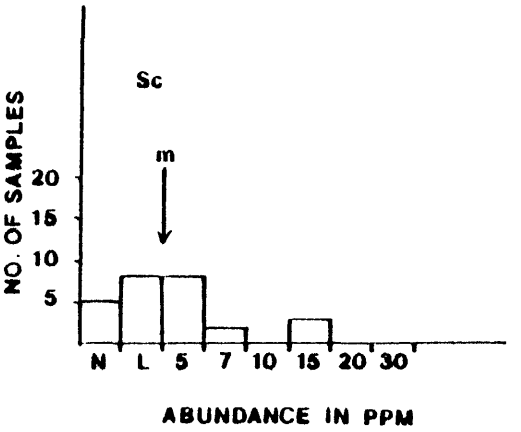

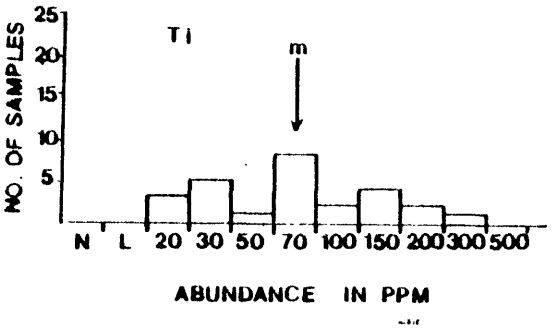

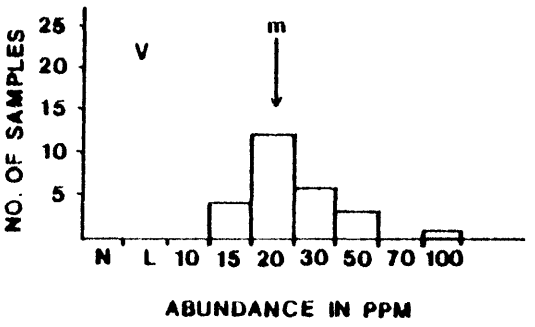

Figure 21.--Continued

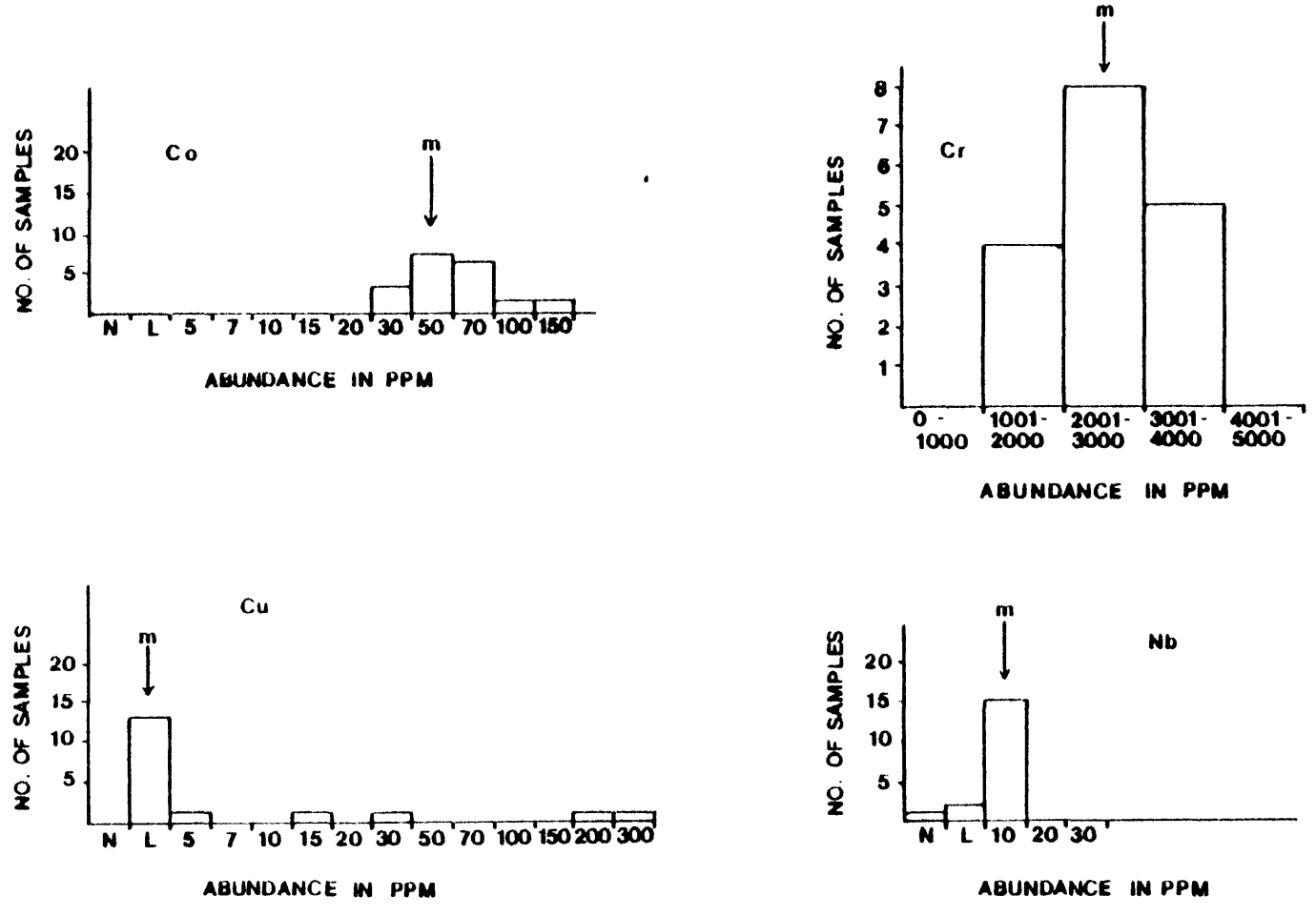

Figure 22.--Histogram of detectable trace elements in wehrlite, Red Mountain ultramafic body, Alaska. Analyses by emission spectrographic methods, except for chromium which was analyzed by atomic absorption (analysts, K. J. Curry and Z. C. Stephenson). m = median.

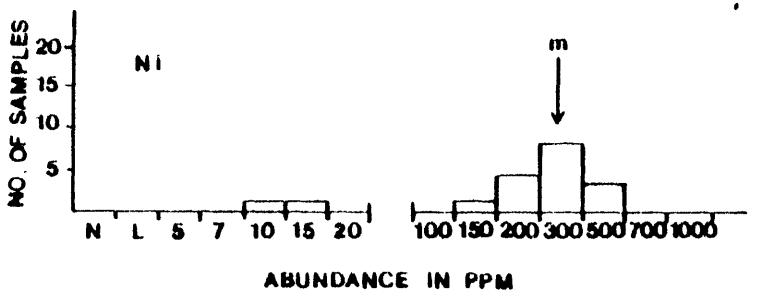

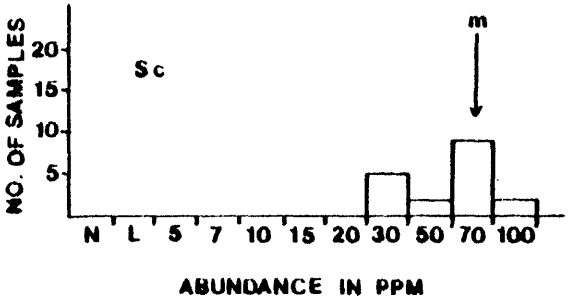

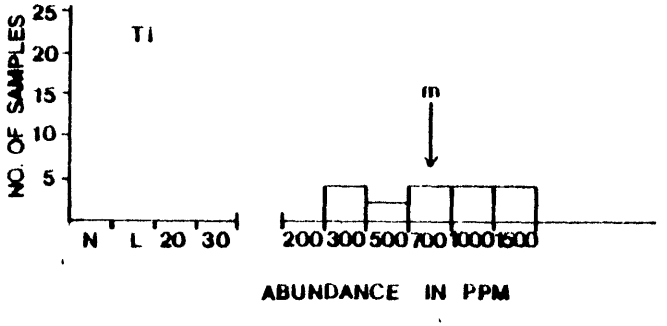

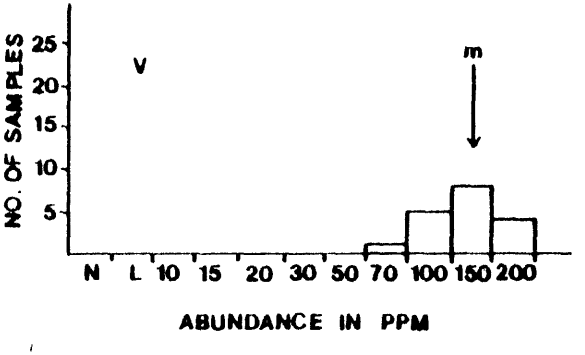

Figure 22.--Continued.

with median values of 4,000-5,000 ppm, 1,800-2,000 ppm, and 150 ppm, respectively. The wehrlites also show high chromium, nickel, and vanadium, but are also richer in scandium and titanium, with median values of 70 ppm and 700 ppm, respectively.

The trace elements iridium, ruthenium, and rhodium were generally not detected in either the dunites or the wehrlites. In the dunite, palladium ranged from not detected at 0.002-0.004 ppm to 0.200 ppm, in one sample. Palladium was higher in the wehrlite, with values from 0.002 to 0.010 ppm. Platinum was not detected in half of the dunite samples, but the remaining samples showed values of 0.005-0.100 ppm; limits of detection were 0.005 to 0.010 ppm. Platinum in the wehrlite ranged from 0.010 to 0.100 ppm.

Petrogenesis

Relict primary textures in the chromitites indicate that the rock formed by cumulus processes. The occurrence of segregated chromite layers has in itself been taken as evidence that the rock differentiated by crystal settling (Thayer, 1970). Thus, the segregated layering of the dunite and wehrlite indicates that these rocks also formed by the processes of crystal settling.

The sequence of layering at Red Mountain is dunite-wehrlite-clinopyroxenite, indicating an apparent order of crystallization of olivine and chromite, followed by olivine, clinopyroxene, and chromite, followed by clinopyroxene alone. These layers commonly form cyclical units; similar sequences are also observed in other layered ultramafic and gabbroic bodies (Jackson, 1971).

Mineral textures from thin-section study indicate that in the dunite olivine formed first followed by chromite. In the wehrlite, olivine and diopside show simultaneous crystallization with traces of chromite being the last primary phase to form. Textures in the clinopyroxenite suggest a similar crystallization order.

Chromite is extremely important as a petrogenic indicator in that it contains five components (FeO, Fe_2O_3, Cr_2O_3, MgO, Al_2O_3) and is thus more responsive to chemical variations occurring within the magma. Chromite generally shows well-developed differentiation trends as outlined by Thayer (1970) and Irvine (1967), and is also physically and chemically more stable than the other silicates with which it occurs.

The liquidus relations in the system $MgO-SiO_2-Cr_2O_3$ roughly approximate the crystallization of chromite from a basaltic magma at low pressures (Keith, 1954). This system shows that picrochromite precipitates with either forsterite or Mg-pyroxene along cotectic boundaries that are close to the $MgO-SiO_2$ join. Liquids that precipitate olivine and (or) pyroxene before chromite contain only a small proportion of Cr_2O_3, approximately 2 percent. This is typical of Red Mountain where dunite is the dominant rock type and chromite is an ubiquitous later phase comprising 1-4 percent of the rock.

The sequence of crystallization at Red Mountain can be modeled by fractional crystallization of the appropriate liquid in the system $Mg_2SiO_4-CaMgSi_3O_6-CaAlSi_2O_8$ (Osborn and Tait, 1952). Osborn and Tait (1952) suggested that the crystallization of chromite is terminated because of a peritectic relation to clinopyroxene. The termination of chromite crystallization and the initiation of diopside crystallization was noted at Duke Island in southeast Alaska, in the lower part of the Muskox intrusion, and near Tulameen, British Columbia (Irvine, 1967). In those examples, chromite is ubiquitous in the dunite and absent from the olivine clinopyroxenite. The Red Mountain rocks also show this trend. Irvine (1967) showed that the initiation of diopsidic crystallization in mafic silicate melts through the chromite to clinopyroxene peritectic relation is determined by the amount of CaO in the melt and is independent of SiO_2. I have previously shown that the Red Mountain diopsides are extremely high in CaO.

The complete absence of orthopyroxene at Red Mountain and in several other ultramafic bodies in southeast Alaska and along the Kodiak-Kenai-Chugach ultramafic belt may be a function of the oxygen fugacity (Irvine, 1967). Irvine (1967) presented a schematic representation of the activity of ferrosilite (fs) in orthopyroxene, clinopyroxene, and wollastonite solid solution coexisting in equilibrium at a specific temperature and pressure with olivine having a fixed intermediate Mg-Fe^{++} ratio. As the activity of ferrosilite is directly related to f_{O_2} (from the equation 3 fayalite + 1/2 O_2 - magnetite + 3 ferrosilite), the precipitation of clinopyroxene over orthopyroxene is favored by a low a_{fs} (this is, high Ca/Ca+Mg) and low f_{O_2}. I have already demonstrated that the pyroxenes at Red Mountain are high-calcium pyroxenes. The lack of primary magnetite in any of the Red Mountain rocks and the high Fe^{2+}/Fe^{3+} in chromite suggest that the oxygen fugacity was also low. These factors may explain why no orthopyroxene is present at Red Mountain and possibly in the other ultramafic exposures along the Kodiak-Kenai-Chugach belt and in southeastern Alaska.

CHAPTER IV

KODIAK-KENAI-CHUGACH ULTRAMAFIC BELT

An arcuate belt of gabbroic and ultramafic bodies is defined from the southwest exposures on Kodiak Island to the easternmost exposures in the Chugach Mountains (fig. 23). Most of these bodies crop out near the Border Ranges thrust fault as mapped by MacKevett and Plafker (1974) and modified by recent data by Beikman (1978). The petrology, structure, and tectonic setting of these bodies are extremely similar (table I), and are discussed below.

Structure

All contacts of the ultramafic bodies with the surrounding country rock are faults that dip steeply inward to vertical. These fault zones are serpentinized and often show extreme brecciation and strong development of slickensides. Most of the bodies are elongate outcrops, commonly parallel to the regional structural trend. Two of the bodies are overturned and evidence for internal faulting and disruption is abundant. The bodies on Kodiak Island, on the southwestern Kenai Peninsula near Seldovia and near Eklutna, intrude the Uyak and McHugh Complexes south of the Border Ranges thrust fault, whereas the Tonsina body, the Wolverine Complex (Carden and Decker, 1977), and the Spirit Mountain complex (informal name) intrude upper Paleozoic to lower Mesozoic metamorphic rocks north of the fault (fig. 23). All these intrusive bodies are close to the Border Ranges fault.

Petrology

All the bodies show well-developed primary igneous layering. Cumulus textures are common, indicating formation by crystal settling and gravity differentiation. Dunite is the prominent lithology; wehrlite and clinopyroxenite are the second most abundant rock types. There is a conspicuous lack of any orthopyroxene-bearing rocks at most of the described

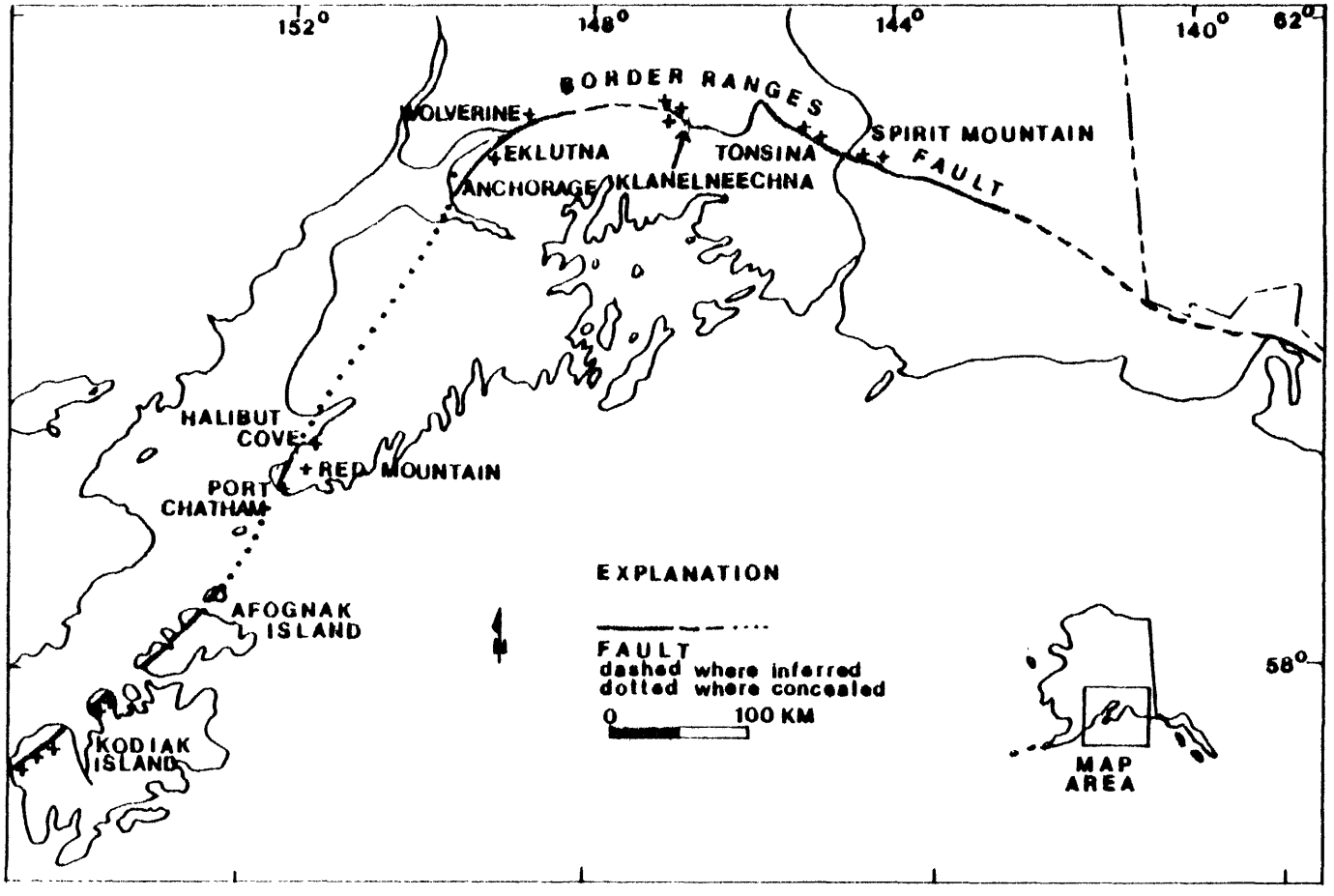

Figure 23.--Outcrops of ultramafic and gabbroic bodies along the Border Ranges fault (+). Modified from MacKevett and Plafker (1974), Rose (1966), Beikman (1978), and Winkler, G. (written commun., 1979).

Table I. Properties of bodies along the Kodiak-Kenai-Chugach ultramafic belt. Sources: Kodiak Island, Connelly (1978) and Nelan (1964); Port Chatam, Gill (1922); Red Mountain, Gill (1922), Child (1942), and work by the author, Halibut Cove, Cowan and Ross (1978) and Cowan (written commun., 1979); Eklutna, Ross (1966); Wolverine, Clark (1972b); Tonsina, Hoffman (1974); Ragan and Grybeck (1965); D. S. Klaneleechema, G. Winkler (written commun., 1979); Spirit Mountain, Kingston and Miller (1945).

Location	Form	Structure	Country rock	Lithology	Texture
Kodiak Island	4 elongate slivers: 10-15 km long, 2 km wide; 1 elliptical body 1 km x 1/2 km	fault-bounded; serpentinized margins	Uyak Complex	layered gabbro, clinopyroxenite, dunite, plagioclase peridotite	
Kenai Peninsula					
1. Port Chatam	irregular	fault-bounded; serpentinized margins	Uyak and McHugh Complexes	layered dunite, chromitite	
2. Red Mountain	elliptical, NE trend 6 km long	fault-bounded; serpentinized margins; steep to vertical contacts; basin structure with SW plunge	Uyak and McHugh Complexes	layered dunite, wehrlite, clinopyroxenite	cumulus with strong deformational overprint
3. Halibut Cove	circular; 1 km diameter	fault-bounded; serpentinized margins	Uyak and McHugh Complexes	layered peridotite pyroxenite, gabbro	
Eklutna	elongate; 16 x 3 km NE trend	fault-bounded; serpentinized margins; steep to vertical contacts; overturned	Upper Paleozoic-Lower Mesozoic metamorphic rocks	layered wehrlite, dunite, augite gabbro, chromitite	
Wolverine	elongate; 8 km long, .8-3.2 km wide; NE trend	fault-bounded; serpentinized margins; steep to vertical contact; overturned	Upper Paleozoic-Lower Mesozoic metamorphic rocks	layered dunite, clinopyroxenite wehrlite	cumulus with overprint of cataclasis
Klaneleechema	discontinuous; irregular	fault-bounded; partially serpentinized	Upper plate Jurassic layered gabbro; lower plate McHugh Complex	dunite, peridotite, gabbro	cumulus with strong cataclasis
Tonsina	4 or 5 bodies; largest 5 km	minor serpentinized margins	Upper Paleozoic-Lower Mesozoic metamorphic rocks	layered dunite; peridotite; clinopyroxenite minor gabbro	cumulus with overprint of cataclasis
Spirit Mountain	Sill-like; discontinuous	concordant to bedding; fault contact; serpentinized margins	Upper Paleozoic-Lower Mesozoic metamorphic rocks	peridotite; dunite	

localities. Chromite is abundant in almost all the terranes, with concentrations being nearly ore grade. Dunite is always the host rock for the chromite. Nickel is correspondingly high both in stream sediments in basins draining the dunite and in the dunite itself. Copper is often found in anomalously high amounts in the clinopyroxenite.

Secondary deformational features that commonly obliterate primary textures are present in many of the ultramafic bodies. Such deformational features include cataclastic textures, recrystallization, and the development of deformation lamellae and undulatory extinction in olivine and diopside. Deformed dunite often shows similar textures with large deformed porphyroclasts of olivine surrounded by a fine-grained recrystallized groundmass.

Due to the similarities in structure, tectonic setting, deformational history, composition, and petrology, I assume that any proposed origin for the Red Mountain ultramafic body must also account for the origin of the other ultramafic bodies exposed along the Kodiak-Kenai-Chugach belt. Because only limited descriptions are available on the Spirit Mountain body, correlation of it with other ultramafic bodies exposed along the ultramafic belt is not certain; its sill-like form and metallic mineralization are atypical of the other ultramafics. For these reasons, I exclude the Spirit Mountain body from consideration until further data on the petrology become available.

CHAPTER V

ORIGIN AND TECTONIC HISTORY

Origin

This chapter is a discussion of the origin, deformation, and probable means of emplacement of the Red Mountain ultramafic body. Several classes of ultramafic bodies outlined by Wyllie (1967, 1970), are based on petrological, structural, and geochemical properties, as well as on the tectonic regime that is unique to that specific type of ultramafic body. Using Wyllie's classification, Red Mountain and similar ultramafics exposed along the Kodiak-Kenai-Chugach belt probably belong to the ophiolite association, dominantly on the basis of their tectonic environment along a paleo-subduction zone and their unique petrological, structural, and geochemical properties.

There is a great deal of controversy over the exact nature of ophiolites and their interpretation as slices of oceanic crust. In 1972 the Geological Society of America sponsored an Internationl Penrose Conference on ophiolites (Penrose Field Conference, 1972), and the definition of ophiolite produced by that conference shall be used here as a basic premise of the present thesis. As defined (Penrose Field Conference, 1972, p. 24-25):

> "Ophiolite refers to a distinctive assemblage of mafic to ultramafic rocks. It should not be used as a rock name or as a lithologic unit in mapping. In a completely developed ophiolite the rock types occur in the following sequence, starting from the bottom and working up: Ultramafic complex, consisting of variable proportions of harzburgite, lherzolite, and dunite, usually with a metamorphic tectonic fabric (more or less serpentinized); Gabbroic complex, ordinarily with cumulus textures commonly containing periodotites and pyroxenites and usually less deformed than the ultramafic complex; mafic volcanic complex, commonly pillowed. Assorted rock types include: (1) overlying sedimentary section typically including ribbon cherts thin shale interbeds, and minor limestone; (2) podiform bodies of chromite generally associated with dunite, and (3) sodic felsic intrusive and extrusive rocks. Faulted contacts between mappable units are common. Whole sections may be missing. An ophiolite may be incomplete, dismembered, or metamorphosed, in which case it should be called a partial

dismembered, or metamorphosed ophiolite. Although ophiolite generally is interpreted to be oceanic crust and upper mantle the use of the term should be independent in its supposed origin."

Throughout the world, ophiolites are typically exposed along belts that show evidence of strong deformation and tectonism. They occur along major sutures that mark the sites of ancient subduction zones and are therefore associated with convergent plate boundaries. Ophiolites are allochthonous features, generally having formed at oceanic spreading ridges, marginal basins, or rift zones, and subsequently emplaced along continental margins. They usually occur in a sheared and chaotic assemblage of sedimentary and metamorphic rocks typical of a melange. Blueschist belts are also a significant feature in these suture zones.

Coleman (1977) estimated that the amount of oceanic crust incorporated into the orogenic zones of continental margins is 0.001 percent of the total oceanic crust formed. The tectonic emplacement of ophiolites is therefore only a minor occurrence and may relate to a rare but major perturbation of plate motions. Ophiolites range from Paleozoic through Cenozoic in age. No Precambrian ophiolites have been unequivocally described although many of the Archean greenstone belts may be remnants of oceanic crust. These belts are autochthonous and formed under conditions that were unique to Archean time.

Metamorphic peridotites form the bulk of ophiolitic sequences, although they are interpreted not to have formed consanguineously with the rest of the ophiolite sequence (Coleman, 1977). It was previously suggested by many workers that metamorphic peridotites represented contemporaneous residual mantle that remained after producing the mafic magma for the overlying cumulate and extrusive rocks. Coleman (1977) interpreted metamorphic peridotites to represent much older parts of the mantle that have moved tectonically upward to form the base upon which the upper section of the

ophiolite developed. This is supported by extremely low levels of incompatible trace elements and high Sr^{87}/Sr^{86} which indicate that the metamorphic peridotites may have undergone partial melting at least 1 b.y. (billion years) ago. The peridotites are chemically homogeneous, suggesting that they are not of cumulate origin where crystal fractionation is a major process. They also exhibit subsolidus recrystallization features that are possible only at mantle pressures and temperatures.

Direct connections between the matamorphic periodotites and overlying cumulates such as feeder dikes or transition zones are unknown. Unconformities separate the two rock types. The underlying metamorphic peridotites are often intensely deformed and folded, whereas the overlying cumulates show no evidence of this deformation (see Jackson and others, 1975). The age difference between the metamorphic peridotites and overlying cumulates is also unknown.

The combination of field and petrologic studies suggest that the Red Mountain ultramafic body may be considered to be a part of a dismembered and metamorphosed ophiolite. Although its severe deformational fabric suggests that it represents a part of the metamorphic peridotite section of an ophiolite, the following criteria (Coleman, 1977) show instead that the Red Mountain ultramafic rocks are a part of the ultramafic cumulate section.

Lithology

Of the two rock types in metamorphic peridotites, harzburgite is more abundant than dunite. Clinopyroxene never exceeds 5 percent by volume. At Red Mountain, dunite is the dominant lithology but wehrlites are common, comprising 10 percent of the rock exposure at Red Mountain. This difference strongly suggests that the lithologies at Red Mountain have affinities closer

to the ultramafic cumulate section of an ophiolite than to the metamorphic peridotite section.

Olivine chemistry

MgO/MgO+FeO*+MnO for olivine from metamorphic peridotites in ophiolites range from 0.87 to 0.945 and have a median value of 0.91; the Red Mountain olivines range from 0.77 to 0.89 with a median value of 0.86 (fig. 24). The Red Mountain olivines clearly are poorer in MgO than are the metamorphic peridotites, but the MgO content is close to that found in ultramafic cumulates in ophiolitic rocks.

Diopside chemistry

The diopside that is typically present in metamorphic peridotites is extremely rich in chromium, averaging 0.67 percent Cr_2O_3. In contrast, the Cr_2O_3 content of Red Mountain diopsides is 0-0.2 percent, with the exception of one sample which contains 0.9 percent Cr_2O_3. The diopside in metamorphic peridotites also has a fairly high Al_2O_3 content ranging from less than 1 percent to greater than 7 percent (Coleman, 1977), whereas the Red Mountain diopside has either no detectable Al_2O_3, or, as in the garnet pyroxenite bodies, abnormally high Al_2O_3. Ca-Ca+Mg atomic ratios of diopside in the metamorphic peridotites range from 39 to 50 percent (Coleman, 1977); those at Red Mountain range from 57 to 59 percent in the wehrlite bodies and from 67 to 69 percent in the garnet clinopyroxenite bodies. The clinopyroxenes in ultramafic cumulates are much more calcic than the metamorphic peridotites.

Cumulate textures

Evidence for cumulate textures in the Red Mountain rocks consists of preserved primary cumulate textures in the chromitite and the presence of

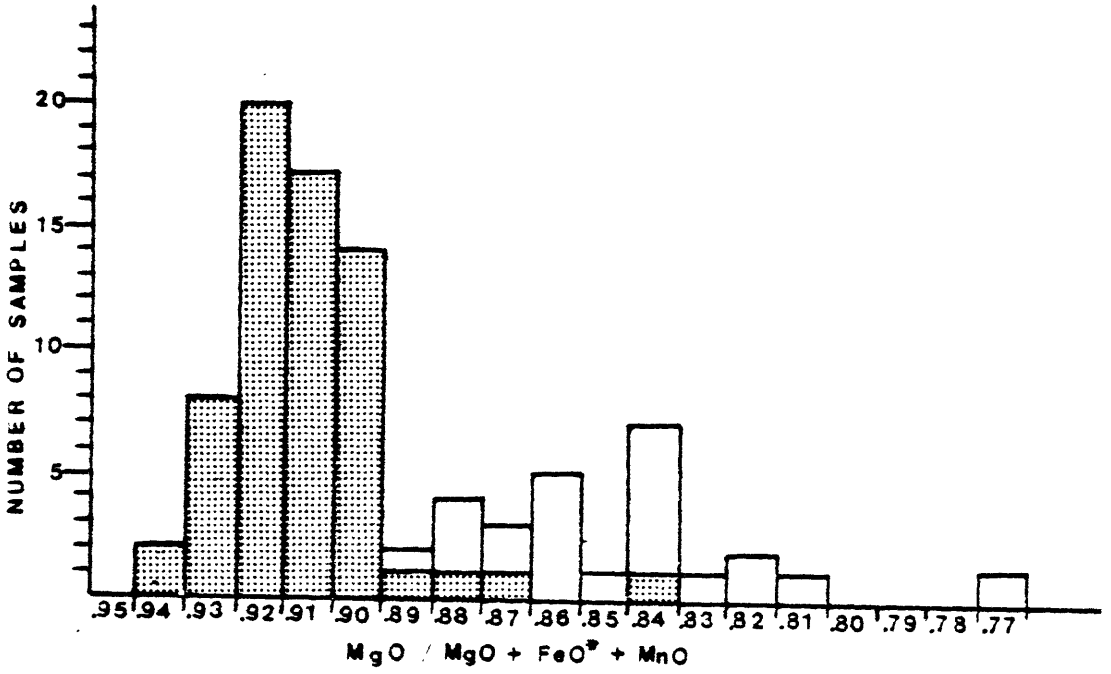

Figure 24.--Histogram showing range in composition of olivines from ophiolite metamorphic peridotites (dotted pattern) (modified from Coleman, 1977) and olivines from Red Mountain.

well-formed, continuous chromitite, wehrlite, and dunite layers. Metamorphic peridotites show no evidence of any cumulate textures.

The whole rock geochemistry of the Red Mountain rocks, the composition of the respective mineral phases, and the presence of cumulate textures, indicate that the Red Mountain ultramafic body is not a remnant of a basal metamorphic peridotite of an ophiolite. Rather, it formed by cumulus processes as a portion of the ultramafic cumulate section that formed at an oceanic spreading center. The other ultramafic bodies exposed along the Kodiak-Kenai-Chugach arc probably were formed along the same spreading center.

The origin of the garnet pyroxenite bodies is uncertain. The bodies clearly have ambiguous textures and a unique chemistry. Experimental work by Green and Ringwood (1967) has established some limiting pressures and temperatures for the stability of the diopside-garnet mineralogy.

Green and Ringwood (1967) made isothermal runs ($1100^{\circ}C$) on an alkali-poor olivine tholeiite glass which is similar in composition to the garnet-pyroxenite bodies at Red Mountain. Their work demonstrated that plagioclase is not stable at pressures greater than 13.5 kb, which may be a lower limiting pressure for the Red Mountain garnet pyroxenites (but only at a temperature of $1,100^{\circ}C$). Because these experiments (Green and Ringwood, 1967) did not show reversals, the phases could be metastable.

Phase data on liquidus relations at elevated pressures and temperatures for rocks similar in composition to the Red Mountain garnet pyroxenites are scarce. Work on garnet-peridotites and the system $CaSiO_3$-$MgSiO_3$-Al_2O_3 is presented by Boyd (1970), Kushiro and others (1967), and O'Hara (1968). O'Hara (1968) suggested that liquids of the composition of the Red Mountain garnet pyroxenites would crystallize at 23 kb and $1,350^{\circ}C$.

Experiments on liquidus and solidus relations of the garnet-diopside system indicate that the mineral assemblage is stable at upper mantle pressures and temperatures. Using these data, two possible origins are herein proposed for the garnet-clinopyroxenite bodies at Red Mountain.

(1) Origin as xenoliths: The garnet pyroxenite bodies may be xenoliths derived from the upper mantle. The bodies could have been incorporated into the Red Mountain pluton either before or after solidification of the body. Yoder (1976) stated that magma generation occurs in broad depth ranges that extend from 50 to 170 km and that may be as deep as 300 km. Because the garnet pyroxenite bodies may have originated in the 50-70 km range, they could have been incorporated into the magma. Yoder (1976) suggested that garnet pyroxenite xenoliths may represent primary mantle, cumulates from liquids produced on partial melting of mantle material, or residual from partial melting; however, that dense xenoliths as large as 90 m across could be carried upward with the magma seems unlikely.

If the bodies were incorporated after solidification of the Red Mountain pluton, they were probably faulted into place during subduction, metamorphism, and emplacement of the Red Mountain pluton into the Seldovia Bay melange. The serpentinized margins of the garnet pyroxenite bodies would ease emplacement.

(2) Origin as dikes: The second possibility for the origin is that the garnet pyroxenite bodies were undersaturated basaltic dikes emplaced into the ultramafic section of the Red Mountain pluton. This type of dike emplacement is commonly observed in the basal part of many ophiolites and is discussed by Coleman (1977). The entire pluton would have to be subjected to the temperatures and pressures discussed for the metamorphism of the garnet pyroxenite bodies.

The garnet pyroxenite bodies show a much greater degree of mechanical deformation than the enclosing pluton. Whereas diopside in the Red Mountain wehrlites and clinopyroxenites shows little deformation, diopside in the garnet pyroxenite bodies shows bending, strong undulatory extinction, and cataclastic textures are common. The garnet is extensively sheared and granulated. On this basis, the garnet pyroxenite bodies most likely are mantle-derived xenoliths, and it is my opinion that the xenoliths were incorporated into the Red Mountain ultramafic after solidification and probably associated with the subduction and emplacement of the body.

Deformational history

Prior to emplacement into the Seldovia Bay complex, the Red Mountain ultramafic body underwent a complex deformation characterized by the development of deformation lamellae and kink bands in individual olivine grains, along with subsolidus recrystallization, polygonalization, and minor cataclasis. Experimental studies on the deformational features found within the dunite may help in delimiting the pressures and temperatures of deformation.

Kink bands in olivine result from inhomogeneous translation gliding in which the amount of translation in the slip plane varies in the direction of slip (Raleigh, 1968). Studies by Raleigh (1963, 1965, 1967, 1968), Carter and Ave'Lallemant (1970), Ave'Lallemant (1975), and Carter (1976) have produced data about the dependence of slip mechanisms in olivine on pressure, temperature, and strain rate. Natural environments are dominated by the {100} (001) mechanism, upper-mantle peridotites are dominated by the {0kl} (100) mechanism, and the high-temperature system {010} (100) is important for some alpine-type peridotites and inclusions in basalts and kimberlites (Mercier and Nicholas, 1975). For representative geological strain rates and for the {100}

(001) mechanism, the temperature of plastic deformation in olivine is 300°C; for lower strain rates this temperature will be correspondingly lower. Limiting pressures are from 1 bar to greater than 65 kb.

Experimental work on recrystallization in olivine has been performed by Raleigh and Kirby (1970), Ave'Lallemant and Carter (1970), and Carter and Ave'Lallemant (1970). In experimentally deformed dunites, polygonalization was first observed at 1,000°C (Carter and Ave'Lallemant, 1970) (for strain rate of 10^{-3} seconds). These temperatures decrease 50°C with a ten-fold reduction in strain rate, and pressure changes have little effect on the temperature. For a representative strain rate of 10^{-14}/second, temperatures of 450°C are indicated for recrystallization and polygonalization of olivine. Recrystallization is the dominant mode of deformation in high-temperature experiments, occurring at higher temperatures than the development of kink bands (Carter and Ave'Lallemant, 1970). The Red Mountain dunites, therefore, probably reached temperatures of 450° for deformation, but this value will be lower with lower strain rates.

It is experimentally known that diopside is structurally more resistant than olivine, and it has been suggested that diopside may behave passively in the deformation of olivine-diopside rocks, resulting in the absence of preferred orientation. Griggs and others (1960), Raleigh (1965), Raleigh and Talbot (1967), and Kirby and Christie (1972) have studied the deformation of diopside in naturally and experimentally deformed tectonites, but no quantitative limits on the temperature, pressure, and strain rate of deformation have been established.

Serpentinization

The contact of the Red Mountain Pluton with the enclosing country rock is a well-developed sheared serpentinite zone. The dunite, and to a lesser

extent the wehrlite, show varying degrees of serpentinization. Assuming that serpentinization involves only olivine and water, the hypothetical reactions representing the most probable chemical changes are as follows:

$$2\ Mg_2SiO_4 + 3H_2O \longrightarrow Mg_3Si_2O_5(OH)_4 + Mg(OH)_2$$

olivine — serpentine — brucite (1)

$$2\ Mg_2SiO_4 + 2H_2O \longrightarrow Mg_3Si_2O_5(OH) + MgO\ (removed)$$

olivine — serpentine (2)

$$3Mg_2SiO_4 + 4H_2O + SiO_2 \longrightarrow 2Mg_3Si_2O_5(OH)_4$$

olivine — serpentine (3)

If the excess MgO in the serpentinization process is used to form brucite (equation 1), then olivine can be converted to serpentine by the addition of water only. Equations (2) and (3) show that olivine cannot be converted to serpentine without the addition of SiO_2 or the subtraction of MgO. If the serpentinization of dunite is accomplished only by the addition of H_2O, the whole-rock MgO-SiO_2 ratio should remain constant. Values for Red Mountain are fairly constant, ranging from 1.13 to 1.23, indicating that the reaction in equation (1) was probably the governing reaction. Further evidence of this is that brucite is also present in many serpentine veins in the dunite at Red Mountain. Volume expansion associated with serpentinization is also common on Red Mountain as indicated by offset grains cut by serpentine.

At least two stages of serpentinization may occur in the Red Mountain dunite. The first occurred slightly before and during the final emplacement of the body as indicated by the brecciated serpentinized margins and the folded serpentine veins. Later serpentinization cut across the folded serpentine veins and was responsible for the formation of most of the serpentine veins. Because serpentine cannot exist at temperatures greater than 500°C (Barnes and O'Neil, 1969), both episodes of serpentinization

probably occurred during and after the actual emplacement of the body into the Seldovia Bay terrane.

Emplacement

As discussed by Coleman (1971), steady-state subduction is required to consume the large amounts of oceanic crust that have formed at oceanic spreading centers. Only by the cessation of steady-state subduction can the oceanic crust become detached and incorporated into the continental margin. Coleman (1977) noted that large, unmetamorphosed ophiolite slabs are present along continental margins which have obviously escaped subduction. He described this process as obduction, the overthrusting of oceanic crust at consumptive plate margins, and he discussed the probable causes for this means of emplacement.

Because the rocks at Red Mountain show a distinct deformational fabric, they were probably not emplaced by obduction. Instead, the ophiolite slab most likely underwent subduction, concomitant with deformation, and was dismembered and emplaced into the melange of the Seldovia Bay terrane. The development of serpentinite margins and internal serpentinization clearly eased emplacement due to the contrasting density (3.3 for dunite versus 2.55 for serpentinite) and the low strength of sheared serpentinite, which has been estimated at 1 bar by Cowan and Mansfield (1970).

The emplacement of the Red Mountain pluton into the Seldovia Bay terrane occurred either before or concurrent with the metamorphism of the enclosing country rock. This interpretation is supported by the similar trends of the axis of the Red Mountain synform and the metamorphic foliation in the Seldovia terrane. Deformational features in the dunite and wehrlite of the Red Mountain pluton also indicate temperatures of metamorphism similar to those of the enclosing Seldovia Bay terrane.

REFERENCES CITED

Ave'Lallemant, H. G., 1975, Mechanisms of preferred orientations of olivine in tectonite peridotites: Geology, v. 3, p. 653-656.

Ave'Lallemant, H. G., and Carter, N. L., 1970, Syntectonic recrystallization of olivine and modes of flow in the upper mantle: Geological Society of America Bulletin, v. 81, p. 2203-2220.

Barnes, I., and O'Neil, J. R., 1969, The relationship between fluids in some fresh alpine-type ultramafics and possible modern serpentinization, Western United States: Geological Society of America Bulletin, v. 80, 1947-1960.

Beikman, H. M., compiler, 1978, Preliminary geologic map of Alaska: U.S. Geological Survey, scale 1:2,500,000, 2 sheets.

Benson, W. N., 1942, The basic igneous rocks of eastern Otago and their tectonic environment: Royal Society of New Zealand Transactions, v. 72, no. 20, p. 113.

Boyd, F. R., 1970, Garnet peridotites and the system $CaSiO_3$-$MgSiO_3$-Al_2O_3: Mineralogical Society of America Special Paper no. 3, p. 65-75.

Burk, C. A., 1965, Geology of the Alaska Peninsula--Island arc and continental margin: Geological Society of America Memoir, no. 99, 250 p.

Carden, J. R., and Decker, J. E., Tectonic significance of the Knik River Schist Terrane, south-central Alaska: Alaska Division of Geological and Geophysical Surveys, Geological Report 55, p. 7-9.

Carden, J. R., Connelly, William, Forbes, R. B., and Turner, D. L., 1977, Blueschists of the Kodiak Islands, Alaska: an extension of the Seldovia schist terrane: Geology, v. 5, p. 529-533.

Carter, N. L., 1976, Steady state flow of rocks: Review of Geophysics and Space Physics, v. 14, p. 301-360.

Carter, N. L., and Ave'Lallemant, H. G., 1970, High temperature flow of dunite and peridotite: Geological Society of America Bulletin, v. 81, p. 2181-2201.

Clague, D. A., and Straley, P. F., 1977, Petrologic nature of the oceanic Moho: Geology, v. 5, p. 133-136.

Clark, S. H. B., 1972a, Reconnaissance bedrock geologic map of the Chugach Mountains near Anchorage, Alaska: U.S. Geological Survey Mineral Investigations Map, MF-350.

_____1972b, The Wolverine complex, a newly discovered layered ultramafic body in the western Chugach Mountains, Alaska: U.S. Geological Survey Open-File Report 522.

_____1973, The McHugh complex of South-Central Alaska: U.S. Geological Survey Bulletin 1372-D, p. D1-D11.

Coleman, R. G., 1971, Plate tectonic emplacement of upper mantle peridotites along continental edges: Journal of Geophysical Research, v. 76, no. 5, p. 1212-1220.

_____1977, Ophiolites - ancient oceanic lithosphere?: New York, Springer Verlag, 229 p.

Connelly, William, Hill, Malcolm, Hill, B. B., and Moore, J. C., 1976, The Uyak Formation, Kodiak Islands, Alaska: an Early Mesozoic subduction zone complex: Geological Society of America Abstracts with Programs, v. 8, p. 364.

Connelly, William, 1978, Uyak complex, Kodiak Islands, Alaska: a Cretaceous subduction complex: Geological Society of America Bulletin, v. 89, p. 755-769.

Cowan, D. S., and Boss, R. F., 1978, Tectonic framework of the southwestern Kenai Peninsula, Alaska: Geological Society of America Bulletin, v. 89, p. 155-158.

Cowan, D. S., and Mansfield, C. F., 1970, Serpentinite flows on Joaquin Ridge, Southern Coast Ranges, California: Geological Society of America Bulletin, v. 81, p. 2615-2628.

Deer, Q. A., Howie, R. A., and Zussman, J., 1975, An introduction to the rock-forming minerals: London, William Clowes and Sons, Ltd., 528 p.

Detterman, R. L., and Hartsock, J. K., 1966, Geology of the Iniskin-Tuxedni region, Alaska: U.S. Geological Survey Professional Paper 512, 78 p.

Forbes, R. B., and Lanphere, M. A., 1973, Tectonic significance of mineral ages of blueschists near Seldovia, Alaska: Journal of Geophysical Research, v. 78, no. 8, p. 1383-1386.

Forbes, R. B., and Swainbank, R. C., 1974, Garnet-clinopyroxenite from the Red Mountain pluton, Alaska: Geological Society of America Bulletin, v. 85, p. 285-292.

Gill, A. C., 1922, Chromite of Kenai Peninsula, Alaska, U.S. Geological Survey Bulletin 742, 52 p.

Grant, U. S., and Higgins, D. F., 1910, Preliminary report on the mineral resources of the southern part of Kenai Peninsula: U.S. Geological Survey Bulletin 442, p. 168-169.

Grantz, Arthur, Thomas, Herman, Stern, T. W., and Sheffey, N. B., 1963, Potassium-argon and lead-alpha ages for stratigraphically bracketed plutonic rocks in the Talkeetna Mountains, Alaska: U.S. Geological Survey Professional Paper 475B, p. 56-59.

Green, D. H., and Ringwood, A. E., 1967a, An experimental investigation of the gabbro-eclogite transformation and some petrologic implications: Geochimica et Cosmochimica Acta, v. 31, p. 767-833.

Griggs, D. T., Turner, F. J., and Heard, H. C., 1960, Deformation of rocks at 500-800°C: Geological Society of America Memoir 79, p. 39-104.

Grimes, D. J., and Marranzino, A. P., 1968, Direct-current arc and alternating-current spark emission spectrographic field methods for the semiquantitative analysis of geologic materials: U.S. Geological Survey Circular 591, 6 p.

Guild, P. W., 1942, Chromite deposits of Kenai Peninsula, Alaska: U.S. Geological Survey Bulletin 931-G, pt. 1, p. 139-175.

Heinrich, E. W., 1965, Microscopic identification of minerals: New York, McGraw-Hill, 414 p.

Hill, B. B., and Brannon, Joyce, 1976, Layered basic and ultra-basic rocks, Kodiak Island, Alaska: the lower portion of a dismembered ophiolite? [abs.]: American Geophysical Union Transactions, v. 57, p. 1027.

Hill, M. D., and Gill, J. B., 1976, Mesozoic greenstones of diverse ages from the Kodiak Islands, Alaska [abs.]: American Geophysical Union Transactions, v. 57, p. 1021.

Hoffman, B. L., 1974, Geology of the Bernard Mountain area, Tonsina, Alaska: Fairbanks, University of Alaska, M.S. thesis, 68 p.

Jackson, E. D., Green, H. W., and Moores, Elridge, 1975, The Vourinos Ophiolite, Greece: cyclic units of lineated cumulates overlying harzburgite tectonites: Geological Society of America Bulletin, v. 86, p. 390-398.

Keith, M. L., 1954, Phase equilibria in the system $MgO-Cr_2O_3-SiO_2$: Journal of American Ceramicist Society, v. 37, p. 490-496.

Kingston, Jack, and Miller, D. J., 1945, Nickel-copper prospect near Spirit Mountain, Copper River region, Alaska: U.S. Geological Bulletin 943C, p. 49-57.

Kirby, S. H., and Christie, J. M., 1972, A comparative study of two modes of deformation twinning in diopside: American Geophysical Union Transactions, v. 53, p. 727.

Kushiro, I., Syono, Y., and Akimoto, S., 1967, Effect of pressure on garnet-pyroxene equilibrium in the system $MgSi_2O_3$-$CaSiO_3$-Al_2O_3: Earth and Planetary Science Letters no. 2, p. 460-464.

MacKevett, E. M., and Plafker, George, 1974, The Border Ranges fault in south-central Alaska: U.S. Geological Survey Journal of Research, v. 2, no. 3, p. 323-329.

Martin, G. C., Johnson, B. L., and Grant, U. S., 1915, Geology and mineral resources of the Kenai Peninsula, Alaska: U.S. Geological Survey Bulletin 587, 243 p.

Mercier, J. C., and Nicolas, A., 1975, Textures and fabrics of upper-mantle peridotites as illustrated by xenoliths from basalts: Journal of Petrology, v. 16, p. 454-487.

Mertie, J. B., Jr., 1919, Chromite deposits in Alaska: U.S. Geological Survey Bulletin 692, p. 265-267.

Moore, J. C., and Connelly, William, 1976, Subduction, arc volcanism, and forearc sedimentation during the Early Mesozoic, southwestern Alaska: Geological Society of America Abstracts with Programs, v. 8, p. 397-398.

Moore, J. C., and Connelly, William, 1977, Mesozoic tectonics of the southern Alaska margin, in Talwani, M., ed., Problems in evolution of island arcs, deep sea trenches, and back-arc basins: Journal of Geophysical Research Special Volume, Maurice Ewing Symposium Volume, series 1, p. 71-82.

Moore, G. W., 1972, Uplifted trench sediments: Southwestern Alaska-Bering Shelf edge: Science, v. 175, p. 1103-1105.

Nockhold, S. R., 1954, Average chemical composition of some igneous rocks: Geological Society of America Bulletin, v. 65, p. 1007-1032.

Nolan, T. B., 1964, Geological Survey Research 1964: U.S. Geological Survey Professional Paper 501A, p. A117.

O'Hara, M. J., 1968, The bearing of phase equilibria studies in synthetic and natural systems on the origin and evolution of basic and ultrabasic rocks: Earth Science Reviews, v. 4, p. 69-133.

Osborn, E. F., and Tait, D. B., 1952, The system diopside-forsterite-anorthite: American Journal of Science, v. 250A, p. 413-433.

Peck, Lee, 1964, Systematic analysis of silicates: U.S. Geological Survey Bulletin 1170, 89 p.

Penrose Field Conference, 1972, Ophiolites: Geotimes, v. 17, p. 24-25.

Ragan, D. M., 1963, Emplacement of the Twin Sisters dunite, Washington: American Journal of Science, v. 261, p. 549-565.

_____1969, Olivine recrystallization textures: Mineralogical Magazine, v. 37, p. 238-240.

Ragan, D. M., and Grybeck, Donald, 1965, Rocks of the basement complex at Tonsina on the north margin of the Chugach Range, Alaska [abs.]: Geological Society of America, Program for the 61st Annual Meeting of the Pacific Coast Section, p. 45.

Raleigh, C. B., 1963, Fabrics of naturally and experimentally deformed olivine: Los Angeles, University of California, Ph. D. thesis, 214 p.

_____1965, Glide mechanisms in experimentally deformed minerals: Science, v. 150, p. 739-741.

Raleigh, C. B., 1967, Plastic deformation of upper mantle silicate minerals: Geophysical Journal, v. 14, p. 45-55.

_____1968, Mechanisms of plastic deformation of olivine: Journal of Geophysical Research, v. 73, p. 5391-5406.

Raleigh, C. B., and Kirby, S. H., 1970, Creep in the upper mantle: Mineralogical Society of America Special Paper 3, p. 113-121.

Raleigh, C. B., and Talbot, J. L., 1976, Mechanical twinning in naturally and experimentally deformed diopside: American Journal of Science, v. 265, p. 151-165.

Reed, B. L., and Lanphere, M. A., 1973, Alaska-Aleutian Range batholith: geochronology, chemistry, and relation to circum-Pacific plutonism: Geological Society of America Bulletin, v. 84, p. 2583-2610.

Rose, A. W., 1966, Geology of chromite-bearing ultramafic rocks near Eklutna, Anchorage Quadrangle, Alaska: Alaska Division of Mines and Minerals, Department of Natural Resources Geological Report 18, 20 p.

Rutledge, F. A., 1946, Exploration of Red Mountain chromite deposits Kenai Peninsula, Alaska: U.S. Bureau of Mines Report of Investigations 3885.

Shapiro, Leonard, 1967, Rapid analysis of rocks and minerals by a single solution method: U.S. Geological Survey Professional Paper 575-B, p. 187-191.

_____1975, Rapid analysis of silicate, carbonate, and phosphate rocks--revised edition: U.S. Geological Survey Bulletin 1401, 76 p.

Spry, Alan, 1969, Metamorphic textures: New York, Pergamon Press, 350 p.

Streckeisen, A. L., chairman, 1973, Plutonic rocks--classification and nomenclature recommended by the IUGS subcommission on the systematics of igneous rocks: Geotimes, v. 18, no. 10, p. 26-30.

Thayer, T. P., 1970, Chromite segregations as petrogenetic indicators, in Visser, D. J. L., and Gruenwaldt, G. von, eds., Symposium on the Bushveld igneous complex and other layered intrusions: Geological Society of South Africa Special Publication 1, p. 380-390.

Wyllie, J. P., ed., 1967, Ultramafic and related rocks: New York, John Wiley and Sons, 464 p.

_____1970, Ultramafic rocks and the upper mantle: Mineralogical Society of America Special Paper 3, p. 3-32.

Yoder, H. S., 1976, Generation of Basaltic magma: Washington, D.C., National Academy of Sciences, 264 p.

APPENDIX

Table 1. Wet chemical analyses of Red Mountain dunites, recalculated to 100 percent after the deletion of water (analyst, Hezekiah Smith). Modal analyses are recalculated to 100 percent with the omission of serpentine. FeO*=total iron as FeO.

Sample No.	301B	302	320	325	330	333	338	338B	340B	340BX	341	342	343X	344X
SiO_2	37.1	39.5	37.7	39.7	38.9	38.8	38.2	41.2	41.1	41.8	41.6	40.0	40.9	41.0
Al_2O_3	.68	.40	.10	.20	.39	.10	.20	.00	.60	.00	.00	.33	.10	.61
Fe_2O_3	3.5	1.7	3.5	2.2	1.6	1.2	1.4	.30	.80	.50	.20	1.4	.80	.50
FeO	6.0	6.5	4.2	6.8	4.6	7.9	7.6	5.8	9.7	7.0	6.6	7.6	7.0	6.6
MgO	44.0	47.9	44.9	47.1	47.0	48.2	47.0	50.2	44.2	48.2	50.5	47.1	49.3	49.6
CaO	.30	.32	.8	.22	.60	.34	.34	.22	2.2	1.5	.20	.41	.30	.65
Na_2O	.00	.00	.02	.00	.00	.00	.00	.00	.00	.00	.00	.00	.00	.00
K_2O	.03	.04	.06	.03	.00	.03	.02	.01	.02	.02	.02	.05	.03	.00
H_2O^+	7.4	2.7	8.3	4.0	5.3	2.1	3.4	.52	.79	.88	.58	2.7	1.2	.66
H_2O^-	.60	.43	.43	.43	.51	.10	.25	.08	.06	.02	.05	.24	.12	.03
TiO_2	.00	.00	.00	.00	.00	.00	.00	.00	.04	.00	.00	.00	.00	.00
P_2O_5	.00	.00	.00	.00	.00	.00	.01	.00	.00	.00	.04	.00	.01	.00
MnO	.16	.14	.13	.15	.11	.16	.15	.11	.19	.13	.12	.15	.13	.12
CO_2	.08	.32	.19	.19	.21	.05	.09	.03	.09	.11	.11	.12	.07	.08
Total	99.85	99.95	100.33	101.02	99.22	98.98	98.66	98.47	99.79	100.16	100.02	100.10	99.96	99.85
SiO_2	40.39	40.80	41.16	41.10	41.64	40.09	40.09	41.84	41.54	42.11	41.86	41.17	41.46	41.35
Al_2O_3	.74	.41	.11	.21	.42	.10	.10	.00	.61	.00	.00	.34	.10	.62
Fe_2O_3	3.81	1.76	3.82	2.28	1.71	1.24	1.24	.30	.81	.50	.20	1.44	.81	.50
FeO	6.53	6.71	4.59	7.04	4.92	8.16	8.16	5.89	9.80	7.05	6.64	7.82	7.10	6.66
MgO	47.90	49.47	49.02	48.76	50.32	49.80	49.80	51.59	44.67	48.56	50.81	48.48	49.98	50.02
CaO	.33	.33	.87	.23	.64	.35	.35	.22	2.22	1.51	.20	.42	.30	.66
Na_2O	.00	.00	.02	.00	.00	.00	.00	.00	.00	.00	.00	.00	.00	.00
K_2O	.03	.04	.07	.01	.00	.03	.03	.01	.02	.02	.02	.05	.03	.00
TiO_2	.00	.00	.00	.00	.00	.00	.00	.00	.04	.00	.00	.00	.00	.00
P_2O_5	.00	.00	.00	.00	.00	.00	.00	.00	.00	.00	.04	.00	.01	.00
MnO	.17	.14	.14	.16	.12	.17	.17	.11	.19	.13	.12	.15	.13	.12
CO_2	.09	.33	.21	.20	.22	.05	.05	.03	.09	.11	.11	.12	.07	.08
Total	99.99	99.99	100.01	100.01	99.99	99.99	99.99	99.99	99.99	99.99	100.00	99.99	99.99	100.01
$\frac{MgO}{MgO+FeO^*+MnO}$	.83	.86	.86	.84	.89	.84	.84	.89	.81	.87	.88	.84	.84	.88
olivine	98.	95.	98.	97.	98.	99.	97.	96.	97.	98.	97.	98.	98.	98.
chromite	2.	5.	2.	3.	2.	1.	3.	4.	3.	2.	3.	2.	2.	2.

Table 1 (Continued)

	346	347	355	359	366	366X	384	388	392	393	397	399	400
SiO_2	40.1	35.0	41.6	35.8	37.5	36.8	37.6	38.8	40.0	40.0	36.8	40.6	38.8
Al_2O_3	.00	.10	.10	.20	1.8	.10	.48	.10	.20	.30	.10	.00	.70
Fe_2O_3	1.7	4.4	.40	4.9	3.5	3.1	2.6	3.1	1.8	1.6	4.5	1.8	1.1
FeO	6.2	3.0	7.8	4.2	4.1	3.9	4.0	4.9	7.4	8.9	5.4	5.6	12.1
MgO	47.9	43.1	49.1	41.0	42.9	44.3	46.2	45.2	47.2	45.5	42.0	48.0	43.7
CaO	.20	.20	.21	.20	1.4	.36	.30	.50	.24	1.0	.52	.30	1.2
Na_2O	.00	.00	.00	.00	.00	.00	.00	.00	.00	.00	.00	.00	.00
K_2O	.01	.00	.00	.01	.00	.03	.01	.00	.00	.05	.05	.00	.04
H_2O^+	3.7	13.0	.51	11.1	8.2	9.1	8.0	5.8	1.6	1.6	9.9	3.2	.72
H_2O^-	.27	.81	.05	.80	.63	.60	.40	.35	.14	.14	.49	.19	.08
TiO_2	.00	.00	.00	.00	.00	.00	.00	.00	.00	.00	.00	.00	.00
P_2O_5	.01	.01	.01	.01	.00	.01	.01	.00	.00	.00	.00	.00	.00
MnO	.14	.12	.14	.15	.13	.12	.12	.13	.18	.18	.16	.11	.23
CO_2	.15	.25	.10	.27	.07	.21	.15	.05	.03	.03	.05	.06	.05
Total	100.38	99.99	100.22	98.64	100.23	98.61	99.87	98.93	98.79	99.30	99.97	99.88	98.72
SiO_2	41.59	40.61	41.71	41.27	41.03	41.38	41.11	41.81	41.21	41.00	41.08	42.08	39.63
Al_2O_3	.00	.12	.10	.23	1.97	.11	.52	.11	.21	.31	.11	.00	.72
Fe_2O_3	1.76	5.11	.40	5.65	3.83	3.49	2.84	3.34	1.85	1.64	5.02	1.87	1.12
FeO	6.43	3.48	7.83	4.84	4.49	4.39	4.37	5.28	7.62	9.12	6.03	5.80	12.36
MgO	49.68	50.01	49.47	47.27	46.94	49.81	50.51	48.72	48.62	46.64	46.89	49.75	44.64
CaO	.21	.23	.21	.23	1.53	.40	.33	.54	.25	1.03	.58	.31	1.23
Na_2O	.00	.00	.00	.00	.00	.00	.00	.00	.00	.00	.00	.00	.00
K_2O	.01	.00	.00	.01	.00	.03	.01	.00	.00	.05	.06	.00	.04
TiO_2	.00	.00	.00	.00	.00	.00	.00	.00	.00	.00	.00	.00	.00
P_2O_5	.01	.01	.01	.01	.00	.01	.01	.00	.00	.00	.00	.00	.00
MnO	.15	.14	.14	.17	.14	.13	.13	.14	.16	.18	.18	.13	.23
CO_2	.16	.29	.10	.31	.08	.24	.16	.05	.07	.03	.06	.06	.01
Total	100.00	100.00	99.97	99.99	100.01	99.99	99.99	99.99	99.99	100.00	100.01	100.00	100.00
$\frac{MgO}{MgO+FeO^*+MnO}$	.86	.86	.84	.87	.86	.88	.88	.85	.84	.82	.82	.87	.77
olivine	98.	99.	98.	96.	97.	97.	98.	98.	98.	97.	97.	96.	95.
chromite	2.	1.	2.	4.	3.	3.	2.	2.	2.	3.	3.	4.	5.

Table 2.- Wet chemical analyses of wehrlites and clinopyroxenites (samples 317 and 377), recalculated to 100 percent after the deletion of water (analyst Hezekiah Smith). Modal analyses are presented for samples with thin sections.
tr. = trace.

Sample No.	307	317	323	324	326	328	331	332	334	341X	344	362	368A	372	377	385	396	398
SiO_2	52.6	51.2	49.6	49.7	50.7	47.4	51.6	49.8	51.0	51.5	52.9	50.3	51.2	52.4	49.7	49.2	51.2	49.2
Al_2O_3	1.4	2.7	1.2	.60	1.7	3.3	2.1	3.4	2.5	.80	1.0	1.2	1.5	2.8	3.2	1.7	1.8	3.1
Fe_2O_3	.90	1.3	1.1	1.0	.90	2.0	.90	1.1	1.2	.70	.60	1.2	1.4	1.0	1.8	1.1	1.1	.90
FeO	2.8	3.4	3.5	3.1	4.5	5.2	4.0	5.8	5.5	3.4	3.5	3.0	2.6	5.3	4.1	4.8	3.9	6.0
MgO	20.9	18.6	23.8	27.2	23.7	24.5	20.2	20.2	19.0	24.4	20.5	23.6	19.8	19.7	18.6	23.6	20.2	21.0
CaO	20.0	21.0	19.5	16.1	18.1	16.4	20.7	18.8	19.29	18.3	20.4	18.2	21.2	18.3	20.1	17.4	20.2	18.6
Na_2O	.05	.03	.03	.06	.03	.01	.04	.06	.03	.00	.02	.00	.00	.01	.00	.03	.00	.05
K_2O	.04	.03	.03	.08	.04	.05	.02	.04	.03	.01	.00	.00	.00	.00	.05	.06	.00	.06
H_2O^+	.50	1.3	1.4	1.3	.52	1.2	.31	.38	.57	.48	1.2	1.6	2.4	.52	2.4	1.2	.95	.67
H_2O^-	.05	.12	.12	.16	.03	.06	.06	.05	.06	.04	.10	.09	.18	.03	.06	.06	.05	.01
TiO_2	.05	.07	.02	.00	.05	.17	.07	.15	.10	.01	.06	.04	.04	.09	.08	.06	.07	.22
P_2O_5	.00	.00	.00	.00	.00	.00	.00	.01	.00	.00	.01	.00	.00	.00	.00	.00	.00	.01
MnO	.09	.11	.11	.09	.12	.14	.13	.15	.13	.09	.10	.10	.11	.10	.15	.13	.11	.14
CO_2	.03	.02	.06	.02	.08	.04	.03	.07	.02	.03	.01	.04	.02	.02	.01	.02	.02	.02
Total	99.41	99.88	100.47	99.41	100.47	100.47	100.16	100.01	99.43	99.76	100.40	99.37	100.45	100.27	100.25	99.16	99.80	100.00
SiO_2	53.23	51.99	50.13	50.74	50.74	47.78	51.71	50.01	51.61	51.89	53.38	51.81	52.31	52.55	50.82	50.15	51.82	49.55
Al_2O_3	1.42	2.76	1.21	.61	1.7	3.33	2.10	3.41	2.53	.81	1.01	1.24	1.53	2.81	3.27	1.73	1.82	3.12
Fe_2O_3	.91	1.32	1.11	1.02	.90	2.02	.90	1.10	1.21	.71	.61	1.24	1.43	1.00	1.84	1.12	1.32	.91
FeO	2.83	3.46	3.54	3.16	4.50	5.24	4.01	5.82	5.57	3.43	3.53	3.09	2.66	5.32	4.19	4.89	3.95	6.04
MgO	21.15	18.88	24.05	27.77	23.72	24.70	20.24	20.29	19.23	24.59	20.69	23.69	20.23	19.75	19.02	24.06	20.45	21.15
CaO	20.24	21.32	19.71	16.44	18.11	16.53	20.24	18.88	19.52	18.44	20.59	18.75	21.66	18.36	20.55	17.74	20.45	18.73
Na_2O	.05	.03	.03	.06	.03	.01	.04	.06	.03	.00	.02	.00	.00	.01	.00	.03	.00	.05
K_2O	.04	.02	.02	.08	.04	.05	.02	.04	.03	.01	.00	.00	.00	.00	.05	.06	.00	.06
TiO_2	.01	.07	.02	.00	.05	.17	.07	.15	.10	.01	.06	.04	.04	.09	.08	.06	.07	.22
P_2O_5	.00	.00	.00	.00	.00	.00	.00	.01	.00	.00	.01	.00	.00	.00	.00	.00	.00	.01
MnO	.09	.11	.11	.09	.12	.14	.13	.15	.13	.09	.10	.10	.11	.10	.15	.13	.11	.14
CO_2	.01	.02	.06	.02	.08	.04	.03	.07	.02	.03	.01	.04	.02	.02	.01	.12	.02	.02
Total	100.0	99.99	99.99	99.99	99.99	100.01	99.99	99.99	99.98	100.01	100.01	100.00	99.99	100.01	99.98	99.99	100.01	100.00
olivine		7.	16.	4.	9.	6.	6.	6.	14.	11.	8.	4.	4.		10.	10.		
diopside		93.	43.	55.	36.	31.	56.	40.	34.	53.	41.	36.	19.		90.	52.		
chromite		tr.	1.	tr.	1.	tr.	tr.	1.	tr.	tr.	tr.	tr.	tr.		tr.	tr.		
groundmass		0.	39.	40.	52.	63.	39.	53.	51.	36.	49.	60.	57.		0.	39.		

Table 3.--Wet chemical analyses of garnet pyroxenites, recalculated to 100 percent after the deletion of water (analyst, N.S. Skinner). Samples RM10 and RM19 from Forbes and Swainbank (1974).
n.d.=not determined.

Sample No.	367	031	031A	032	RM10	RM19
SiO_2	41.0	42.7	42.7	45.9	39.38	41.47
Al_2O_3	16.9	16.8	16.8	10.6	17.75	17.80
Fe_2O_3	1.7	2.5	2.7	3.7	3.20	3.19
FeO	10.3	10.6	10.2	5.5	11.58	8.79
MgO	9.70	10.0	9.8	10.6	10.21	11.10
CaO	16.5	14.5	15.5	22.1	15.23	15.40
Na_2O	.12	.32	.36	.35	.11	.53
K_2O	.00	.06	.00	.00	.02	.02
H_2O^+	2.3	1.5	1.5	1.2	1.35	1.34
H_2O^-	.23	.40	.39	.17	.05	.05
TiO_2	.49	.61	.56	.99	1.05	.58
P_2O_5	.01	.07	.08	.09	.02	tr
MnO	.26	.18	.18	.08	.23	.21
CO_2	.05	.03	.05	.01	n.d.	n.d.
Total	99.56	100.27	100.82	101.29	100.18	100.48
SiO_2	42.25	43.41	43.16	45.94	39.86	41.84
Al_2O_3	17.42	17.08	16.98	10.61	17.97	17.96
Fe_2O_3	1.75	2.54	2.73	3.7	3.24	3.22
FeO	10.62	10.77	10.31	5.5	11.72	8.87
MgO	10.0	10.16	9.91	10.61	10.34	11.20
CaO	17.01	14.74	15.67	22.12	15.42	15.54
Na_2O	.12	.33	.36	.35	.11	.54
K_2O	.00	.06	.00	.00	.02	.02
TiO_2	.50	.62	.57	.99	1.06	.59
P_2O	.01	.07	.08	.09	.02	tr
MnO	.26	.18	.18	.08	.23	.22
CO_2	.05	.03	.05	.01	n.d.	n.d.
Total	99.99	99.99	100.00	100.00	99.99	100.00
garnet	59.	60.	57.	35.	51.	59.
diopside	41	38	42	65	46	24
amphibole	0	2	1	0	3	17

Table 4.--Microprobe analyses of olivine (by the author). n.d. = not detected.

Rock type--------	wehrlite	dunite	chromitite
Sample No.-------	341X	342	030
SiO_2	39.3	38.9	39.2
Al_2O_3	0.	0.	0.
FeO	10.6	9.5	4.9
MgO	48.6	49.9	54.6
CaO	.2	0.	0.
Na_2O	n.d.	n.d.	n.d.
Total	98.7	98.3	98.7
$MgO/MgO+FeO^+$	.82	.84	.92

Table 5.--Microprobe analyses of chromite (by the author).

Rock type ----------	dunite	chromitite
Sample No.----------	342X	030
SiO_2	1.2	1.0
Al_2O_3	13.0	8.9
FeO	33.5	21.2
MgO	6.5	10.4
CaO	.5	.4
Cr_2O_3	44.5	54.4
Total	99.2	96.3

Table 6.--Microprobe analyses of diopside (by the author) with end member calculations based on six oxygens. Samples RM10 and Rm19 are from mineral separates from Forbes and Swainbank (1974). n.d.= not determined. En=enstatite, Fs=ferrosilite, Wo=wollastonite, CaTs=Tschermaks molecule.

Rock type---wehrlite	clinopyroxenite	----------garnet clinopyroxenite-------			
Sample No.-- 341X	377	032	031A	RM10	RM19
SiO_2 55.1	54.0	47.5	48.3	48.19	47.69
Al_2O_3 0.0	0.0	6.6	7.0	7.00	8.29
Fe_2O_3				2.42	2.53
FeO 2.0	3.7	7.6	6.1	3.84	2.87
MgO 18.2	17.0	11.8	12.9	13.14	12.80
CaO 24.3	24.0	24.0	23.9	24.08	23.76
Na_2O n.d.	n.d.	n.d.	n.d.	0.23	0.43
K_2O 0.0	0.0	0.0	0.0	0.02	0.02
TiO_2 0.1	0.1	0.7	0.6	0.87	1.06
Cr_2O_3 0.9	0.2	0.0	0.0	0.00	0.00
Total . 100.6	99.9	98.2	98.8	99.79	99.45
En 49.4	46.8	32.9	37.1	36.0	35.3
Fs 3.0	6.0	12.9	4.6	9.4	8.6
Wo 47.6	47.3	40.7	42.8	39.9	38.3
CaTs 0.0	0.0	14.5	15.5	14.8	17.9
Total 100.0	100.1	100.0	100.0	100.1	100.1

Table 7.-- Microprobe analyses of garnet (by the author). Samples RM10 and RM19 are wet chemical analyses from mineral separates from Forbes and Swainbank (1974). End member calculations indeterminable for the microprobed samples because the Fe^{++}/Fe^{+++} is unknown. n.d. = not determined.

Sample No.	031	031A	032	RM10	RM19
SiO_2	38.2	42.4	36.1	38.88	39.14
Al_2O_3	25.3	24.0	29.0	21.88	22.38
Fe_2O_3	17.3	4.8	5.6	3.11	4.13
FeO				13.79	11.65
MgO	9.1	6.2	3.4	8.45	9.09
CaO	13.2	20.7	22.8	13.11	12.84
Na_2O	n.d	n.d	n.d	.02	.04
K_2O	n.d	n.d	n.d	.02	.03
Cr_2O_3	n.d	n.d	n.d	.0008	.016
Total	103.1	98.1	96.9	99.26	99.32
Pyrope				33.01	36.28
Grossular				27.33	24.36
Almandine				29.91	26.10
Andradite				9.11	12.49
Spessartine				0.64	0.77

Table 8.--Semiquantitative emission spectrographic analyses for the dunites (analyst, K. J. Curry).
G = greater than the value shown, L= detected, but below limit of determination,
N = not detected at limit of detection. Values along top row indicate the limit of detection for each element.

	Percent				ppm										
Sample No.	0.05 Fe	0.02 Mg	0.05 Ca	0.002 Ti	10 Mn	.5 Ag	200 As	10 Au	10 B	20 Ba	1 Be	10 Bi	20 Cd	5 Co	10 Cr
301B	10	G(10)	.15	.015	700	N	N	N	L	N	N	N	N	150	G(5000)
302	7	G(10)	.15	.003	700	N	N	N	L	N	N	N	N	100	5000
323	10	G(10)	.2	.007	1000	N	N	N	L	N	L	N	N	100	G(5000)
325	15	G(10)	1.5	.02	1000	N	N	N	L	N	N	N	N	150	G(5000)
330	7	10	.3	.007	1000	N	N	N	L	N	N	N	N	150	G(5000)
333	10	G(10)	.2	.003	1000	N	N	N	L	N	N	N	N	150	1500
338B	7	G(10)	.15	.02	700	N	N	N	L	N	L	N	N	100	G(5000)
340B	15	G(10)	1.	.03	1000	N	N	N	L	N	N	N	N	150	G(5000)
340BX	10	G(10)	.7	.007	700	N	N	N	L	N	N	N	N	150	5000
341	7	G(10)	.07	.003	700	N	N	N	L	N	N	N	N	150	2000
342	10	G(10)	.15	.003	1000	N	N	N	L	N	N	N	N	150	3000
343X	10	G(10)	.15	.007	700	N	N	N	L	N	N	N	N	150	G(5000)
344X	7	G(10)	.3	.01	1000	N	N	N	L	N	L	N	N	100	G(5000)
346	10	G(10)	.15	.005	1000	N	N	N	L	N	N	N	N	150	5000
347	10	G(10)	.15	.007	1000	N	N	N	L	N	N	N	N	150	5000
355	10	G(10)	.15	.002	1000	N	N	N	L	N	N	N	N	100	3000
359	10	10	.15	.007	1000	N	N	N	L	N	N	N	N	150	G(5000)
366	7	10	.3	.01	700	N	N	N	L	N	N	N	N	100	G(5000)
366X	10	G(10)	.15	.007	700	N	N	N	L	N	N	N	N	150	G(5000)
384	7	G(10)	.1	.002	700	N	N	N	L	N	N	N	N	150	G(5000)
388	10	G(10)	.3	.015	1000	N	N	N	L	N	N	N	N	150	G(5000)
392	7	G(10)	.1	.003	700	N	N	N	L	N	N	N	N	100	5000
393	7	10	.3	.015	700	N	N	N	70	N	N	N	N	100	3000
397	10	G(10)	.3	.007	1000	N	N	N	L	N	N	N	N	150	3000
399	7	G(10)	.2	.002	700	N	N	N	L	N	N	N	N	150	5000
400	15	G(10)	1.0	.015	1000	N	N	N	L	N	N	N	N	150	5000

Table 8 (continued)

Sample No.	5 Cu	10 La	5 Mo	10 Nb	5 Ni	10 Pb	100 Sb	5 Sc	10 Sn	100 Sr	10 V	50 W	10 Y	200 Zn	10 Zr
	ppm														
301B	5	N	N	10	1500	N	N	7	N	N	100	N	N	N	N
302	L	N	N	10	1000	N	N	5	N	N	20	N	N	N	N
320	L	N	N	10	2000	N	N	L	N	N	30	N	N	N	N
325	L	N	N	10	3000	N	N	15	N	N	50	N	N	N	N
330	L	N	N	10	3000	N	N	L	N	N	20	N	N	N	N
333	L	N	N	10	1500	N	N	L	N	N	15	N	N	N	N
338B	L	N	N	10	3000	N	N	N	N	N	50	N	N	N	N
340B	5	N	N	10	1500	N	N	15	N	N	30	N	N	N	N
340BX	L	N	N	10	2000	N	N	5	N	N	15	N	N	N	N
341	L	N	N	10	2000	N	N	N	N	N	15	N	N	N	N
342	L	N	N	10	1500	N	N	N	N	N	15	N	N	N	N
343X	L	N	N	10	1500	N	N	5	N	N	20	N	N	N	N
344X	L	N	N	10	3000	N	N	L	N	N	20	N	N	N	N
346	L	N	N	10	1500	N	N	5	N	N	20	N	N	N	N
347	L	N	N	10	3000	N	N	5	N	N	20	N	N	N	N
355	L	N	N	10	2000	N	N	L	N	N	20	N	N	N	N
359	L	N	N	10	1500	N	N	L	N	N	30	N	N	N	N
366	N	N	N	10	1000	N	N	5	N	N	30	N	N	N	N
366X	N	N	N	10	3000	N	N	5	N	N	20	N	N	N	N
384	L	N	N	10	1000	N	N	L	N	N	20	N	N	N	N
388	L	N	N	10	700	N	N	L	N	N	30	N	N	N	N
392	L	N	N	10	1000	N	N	N	N	N	20	N	N	N	N
393	L	N	N	10	1500	N	N	N	N	N	20	N	N	N	N
397	L	N	N	10	2000	N	N	7	N	N	30	N	N	N	N
399	L	N	N	10	2000	N	N	5	N	N	20	N	N	N	N
400	L	N	L	10	1500	N	N	15	N	N	50	N	N	N	N

Table 9.--Semiquantitative emission spectrographic analyses for wehrlite, clinopyroxenite (samples 317 and 377), and garnet clinopyroxenite (sample 367) (analyst K.J. Curry). G = greater than the value shown, L = detected, but below the limit of determination, N = not detected at limit of detection. Top row of values indicates the limit of detection for each element.

	Percent				ppm										
Sample No.	0.05 Fe	0.02 Mg	0.05 Ca	0.002 Ti	10 Mn	.5 Ag	200 As	10 Au	10 B	20 Ba	1 Be	10 Bi	20 Cd	5 Co	10 Cr
307	3	10	10	.03	700	N	N	N	N	N	N	N	N	30	5000
317	5	10	15	.15	700	N	N	N	L	N	N	N	N	30	3000
323	7	G(10)	15	.05	700	N	N	N	L	N	N	N	N	70	5000
324	7	10	10	.03	700	N	N	N	N	N	N	N	N	70	3000
326	5	10	10	.05	700	N	N	N	L	N	N	N	N	50	3000
328	10	10	10	.15	1000	N	N	N	L	N	N	N	N	100	3000
331	7	10	10	.10	1000	N	N	N	L	N	N	N	N	70	5000
332	10	10	15	.15	1000	N	N	N	L	N	N	N	N	70	3000
334	5	10	10	.10	1000	N	N	N	L	N	L	N	N	50	3000
341X	5	10	15	.03	700	N	N	N	L	N	N	N	N	70	3000
344	5	10	15	.07	700	N	N	N	L	N	N	N	N	50	5000
362	5	10	15	.03	700	N	N	N	L	N	N	N	N	70	5000
368A	5	10	15	.07	1000	N	N	N	L	N	N	N	N	50	5000
372	5	10	20	.10	700	N	N	N	L	N	N	N	N	30	3000
377	5	10	7	.07	1000	N	N	N	L	N	N	N	N	50	3000
385	7	G(10)	10	.07	1000	N	N	N	L	N	N	N	N	150	3000
396	7	10	10	.10	1000	N	N	N	L	N	N	N	N	50	3000
398	7	10	10	.15	1000	N	N	N	L	N	N	N	N	50	1500
367	10	7	15	.3	1500	N	N	N	10	70	N	N	N	70	700

Table 9 (continued)

Sample No.	5 Cu	20 La	5 Mo	10 Nb	5 Ni	10 Pb	100 Sb	5 Sc	10 Sn	100 Sr	10 V	50 W	10 Y	200 Zn	10 Zr
	ppm														
307	L	N	N	10	300	N	N	30	N	N	100	N	N	N	N
317	L	N	N	10	200	N	N	70	N	N	200	N	N	N	N
323	30	N	N	10	500	N	N	30	N	N	100	N	N	N	N
324	L	N	N	10	300	N	N	30	N	N	70	N	N	N	N
326	L	N	N	10	300	N	N	30	N	N	150	N	N	N	N
328	L	N	N	10	500	N	N	70	N	N	150	N	N	N	N
331	L	N	N	10	200	N	N	70	N	N	150	N	N	N	N
332	15	N	N	10	300	N	N	70	N	N	150	N	N	N	N
334	5	N	N	10	300	N	N	70	N	N	150	N	N	N	N
341X	L	N	N	10	300	N	N	30	N	N	100	N	N	N	N
344	L	N	N	10	300	N	N	70	N	N	100	N	N	N	N
362	L	N	N	10	500	N	N	50	N	N	100	N	N	N	N
368A	L	N	N	10	300	N	N	70	N	N	150	N	N	N	N
372	L	N	N	L	150	N	N	100	N	N	200	N	N	N	N
377	300	N	N	L	15	N	N	50	N	N	200	N	N	N	N
385	L	N	N	N	10	N	N	70	N	N	150	N	N	N	N
390	L	N	N	10	300	N	N	70	N	N	150	N	N	N	N
398	200	N	N	10	200	N	N	100	N	N	200	N	N	N	N
367	15	N	N	10	100	N	N	10	N	150	300	N	10	N	N

Table 10.--Atomic absorption analyses of dunites and wehrlites for chromium and of dunites for nickel (analyst Z.C. Stephenson). n.d. = not determined.

Sample No.	Dunites		Sample No.	Wehrlites
	ppm Cr	ppm Ni		ppm Cr
301B	16000	n.d.	307	3200
302	4400	n.d.	317	1800
320	6400	n.d.	323	2600
325	6200	1300	324	2400
330	6400	1500	326	2600
333	n.d.	1900	328	1200
338B	n.d.	n.d.	331	3200
340B	3800	n.d.	332	1200
340BX	3200	n.d.	334	3200
341	n.d.	2100	341X	2800
342	5400	2200	344	3000
343X	4400	n.d.	362	3200
344X	4400	n.d.	368A	3200
346	7000	n.d.	372	2200
347	3600	n.d.	377	1800
355	3600	1700	385	2600
359	3600	2100	396	2200
366	9200	n.d.	398	n.d.
366X	3800	n.d.		
384	4600	2200		
388	5600	n.d.		
392	5400	n.d.		
393	4200	n.d.		
397	4400	n.d.		
399	4200	1600		
400	3200	1900		

Table 11.--Elemental abundances in parts per million of platinum (Pt), palladium (Pd), rhodium (Rh), ruthenium (Ru), and iridium (Ir) in the dunites (analysts R.R. Carlson and E.F. Cooley). Method of analyses by fire assay.
L = detected, but below limit of determination;
N = not detected at limit of determination.

Sample No.	Pt	Pd	Rh	Ru	Ir
301B	N(.005)	.003	N(.002)	N(.100)	N(.100)
302	.005	.002	N(.002)	N(.100)	N(.100)
320	N(.010)	N(.004)	N(.004)	N(.200)	N(.100)
325	.020	N(.004)	N(.004)	N(.200)	N(.200)
330	N(.010)	N(.004)	N(.004)	N(.200)	N(.200)
338	N(.010)	N(.004)	N(.004)	N(.200)	N(.200)
340B	.030	.020	N(.004)	N(.200)	N(.200)
340BX	N(.010)	N(.004)	N(.004)	N(.200)	N(.200)
341	.015	N(.002)	N(.002)	N(.100)	N(.100)
342	.020	.007	N(.002)	N(.100)	N(.100)
343	N(.010)	N(.004)	N(.004)	N(.200)	N(.200)
344X	N(.010)	N(.004)	N(.004)	N(.200)	N(.200)
346	.020	N(.004)	N(.004)	N(.200)	N(.200)
347	N(.010)	N(.004)	N(.004)	N(.200)	N(.200)
355	N(.005)	.003	N(.002)	N(.100)	N(.100)
359	.015	N(.004)	N(.004)	N(.200)	N(.200)
366	.010	N(.004)	N(.004)	N(.200)	N(.200)
366X	.010	.200	N(.004)	N(.200)	N(.200)
384	.050	N(.004)	N(.004)	N(.200)	N(.200)
388	N(.010)	N(.004)	N(.004)	N(.200)	N(.200)
392	N(.010)	N(.004)	N(.004)	N(.200)	N(.200)
393	N(.005)	N(.002)	N(.002)	N(.100)	N(.100)
397	.030	.020	N(.002)	N(.100)	N(.100)
399	.030	N(.004)	N(.004)	N(.200)	N(.200)
400	.020	.010	N(.002)	N(.100)	N(.100)

Table 12.--Elemental abundances in parts per million of platinum(pt), palladium (pd), rhodium (Rh), ruthenium (Ru), and iridium (Ir) in the wehrlites (analysts R.R. Carlson and E.F. Cooley). Method of analyses by fire assay.
L = detected, but below limit of determination;
N = not detected at limit of determination.

Sample No.	Pt	Pd	Rh	Ru	Ir
323	L(.010)	.003	N(.004)	N(.200)	N(.200)
324	.005	.002	N(.002)	N(.100)	N(.100)
326	.015	.005	N(.002)	N(.100)	N(.100)
328	.050	.030	N(.002)	N(.100)	N(.100)
331	.010	.020	N(.004)	N(.200)	N(.200)
334	L(.005)	.010	N(.002)	N(.100)	N(.100)
341X	.015	.007	N(.002)	N(.100)	N(.100)
344	.010	N(.004)	N(.004)	N(.200)	N(.200)
362	.010	N(.004)	N(.004)	N(.200)	N(.200)
368A	N(.025)	N(.010)	N(.010)	N(.500)	N(.500)
385	.020	.010	N(.002)	N(.100)	N(.100)